Contribution from the Department of Chemistry and the Center of Information Science, University of Auckland, Private Bag, Auckland, New Zealand, Research School of Chemistry, The Australian National University, G.P.O. Box 4, Canberra, ACT 2601, Australia, and Department of Chemistry, Private Bag, University of Canterbury, Christchurch, New Zealand

Relativistic Effects in Gold Chemistry. 3. Gold(I) Complexes

Peter Schwerdtfeger,*,† Peter D. W. Boyd, Anthony K. Burrell, Ward T. Robinson,‡ and Michael J. Taylor

Received November 1, 1989

Geometry-optimized Hartree-Fock (HF) calculations have been carried out for the ground-state properties of linear two-coordinated gold(I) complexes, AuL_2^- (L = H, F, Cl, Br, I, CN, SCN, CH_3, and PH_3^+), and for $AuCH_3$, $AuPH_3$, $AuPH_3^+$, AuCN, and AuSCN by using multielectron adjusted nonrelativistic and relativistic pseudopotentials for the gold atom. Configuration interaction calculations have been performed for the gold(I) halide complexes. The relativistic effects in the Au-L bond are analyzed, and the differences from the corresponding Cu-L and Ag-L bonds are explained. The preference of coordination number 2 in Au(I) is strengthened by relativistic effects. In contrast to singly bonded AuL species (*J. Chem. Phys.* **1989**, *91*, 1762), 5d and 6p contributions to the Au-L bond are important in Au(I) complexes. The magnitude of these effects is dependent on the electronegativity of the ligand. Relativistic effects increase gold 5d contributions in the Au-L bond, as expected from the relativistic expansion of the Au 5d orbital and the relativistic contraction of the Au 6s orbital. In contrast to the diatomics, no significant relativistic bond destabilization was found for the complex halides. Large relativistic bond stabilizations were obtained for $Au(PH_3)_2^+$ and for $Au(CN)_2^-$ (87 and 39 kJ mol^{-1} per Au-L bond at the HF level, respectively), which account for their high stability compared to the analogous copper or silver compounds. The unusually large negative ^{35}Cl nuclear quadrupole coupling constant in $AuCl_2^-$ compared with $CuCl_2^-$ and $AgCl_2^-$ is caused by relativistic effects. Relativistic difference density plots are shown for AuH_2^-, AuF_2^-, and $Au(CN)_2^-$. AuSCN and $Au(SCN)_2^-$ are predicted to have a bent Au-S-C conformation. Since structural data on $Au(SCN)_2^-$ were not available, we have synthesized $[AsPh_4]Au(SCN)_2$ and analyzed this compound by infrared and Raman spectroscopy and have determined its structure by single-crystal X-ray diffraction. These studies confirm the calculated nonlinear Au-S-C arrangement of the $Au(SCN)_2^-$ ion.

I. Introduction

The most common structure observed for gold compounds in the oxidation state +1 is the linear AuL_2^- complex (L = Cl, CN, ...).[1] Au(I) is known to be a very soft Lewis acid that prefers to bind to polarizable ligands such as I^- or CN^-. For example, although AuF_2^- has not yet been reported, both $AuCl_2^-$ and $AuBr_2^-$ have been shown to dissolve in water with disproportionation to AuL_4^- (L = Cl, Br) and gold metal, whereas AuI_2^- is considerably more stable in solution.[1] The $Au(CN)_2^-$ ion is probably the most stable Au(I) complex known and has been studied in detail.[1,2] In contrast, the $Au(SCN)_2^-$ ion has not been studied extensively and the molecular structure is unknown.[2] Although several infrared and Raman studies have been carried out on $Au(SCN)_2^-$,[3-6] it is still not known whether the Au-S-C fragment is linear or bent. Vibrational studies on group 11 complexes[1,2] show an unexpected ordering of the M-L (M = Cu, Ag, Au; L = Cl^-, Br^-, I^-, CN^-) stretching force constants, viz. $k_e(Au-L) > k_e(Cu-L) > k_e(Ag-L)$ (see Figure 1). It has been suggested[1,2] that this trend reflects the increased covalency in the Au(I)-ligand bond. However, increased force constants are also seen in compounds where the Au-L bond is more ionic when compared to the analogous copper or silver species, e.g. in diatomic alkali-metal-gold compounds.[7] The trend in stability constants for AuL_2^- complexes is often given by L = Cl < Br < I $\ll$ CN, but it is not known if this simply reflects the bond stability of such compounds or if other (kinetic or thermodynamic) factors play an important role. The tendency to form such complexes within the group 11 series is Au > Ag $\sim$ Cu and it has often been suggested[1] that the involvement of the fully occupied $5d_\sigma$ core orbitals as well as the virtual $6p_\sigma$ valence orbitals plays a major role in this trend. However, there is still debate on whether the bonding in AuL_2^- complexes should be described by sd or sp mixing.[1a,c]

It was shown in the first paper of this series[7] that relativistic effects significantly change the physical and chemical behavior of such compounds; e.g., the Au-L bond is destabilized by electronegative ligands and stabilized by electropositive ligands. Calculated force constants are drastically increased by the inclusion of relativistic effects, in many cases by more than 50% (see also ref 8). Au(5d) contributions were found to be small and 6p contributions negligible in the Au-L bond. It was suggested that this may change for AuL_2^- compounds; e.g., the destabilizations for the complex gold halides should be less dramatic since 5d or 6p participation in the bond should lead to stabilization. In the second paper of this series,[9] we showed that relativistic effects strongly influence the Au(I)/Au(III) redox behavior in the halide complexes AuL_4^-.

There have been only a few theoretical studies of Au(I) complexes.[10-17] Zwanziger et al. studied the halide complexes of Au(I) using a semiempirical SCCC method (self-consistent charge and configuration approximation).[10] Guenzburger and Ellis studied

† The Australian National University.
‡ University of Canterbury.

(1) (a) Puddephatt, R. J. *The Chemistry of Gold*; Elsevier: Amsterdam, 1978. (b) Puddephat, R. J. In *Comprehensive Organometallic Chemistry*; Wilkinson, G., Stone, F. G. A., Abel, E. W., Eds.; Pergamon: Oxford, England, 1982; Vol. 15, p 765. (c) Puddephatt, R. J. In *Comprehensive Coordination Chemistry*; Pergamon: Oxford, England, 1987; Vol. 5, p 861. (d) Uson, R.; Laguna, A. *Coord. Chem. Rev.* **1986**, *70*, 1. (e) Melnik, M.; Parish, R. V. *Coord. Chem. Rev.* **1986**, *70*, 157.
(2) Bowmaker, G. A. In *Spectroscopy of Inorganic-based Materials*; Clark, R. J. H., Hester, R. E., Eds.; Wiley: New York, 1987; p 1.
(3) Rogers, D. A. Thesis, Department of Chemistry, University of Auckland, Auckland, NZ, 1980.
(4) Ellestad, O. H.; Klaeboe, P.; Tucker, E. E.; Sengstad, J. *Acta Chem. Scand.* **1972**, *26*, 3579.
(5) Bowmaker, G. A.; Rogers, D. A. *J. Chem. Soc., Dalton Trans.* **1982**, 1873.
(6) Melpolder, J. B.; Burmeister, J. L. *Inorg. Chim. Acta* **1981**, *49*, 115.
(7) Schwerdtfeger, P.; Dolg, M.; Schwarz, W. H. E.; Bowmaker, G. A.; Boyd, P. D. W. *J. Chem. Phys.* **1989**, *91*, 1762.
(8) (a) Pyykkö, P. *Chem. Rev.* **1988**, *88*, 563. (b) Pyykkö, P. *Adv. Quantum Chem.* **1978**, *11*, 353.
(9) Schwerdtfeger, P. *J. Am. Chem. Soc.* **1989**, *111*, 7261.
(10) Zwanziger, H.; Reinhold, J.; Hoyer, E. *Z. Chem.* **1974**, *14*, 489.
(11) Guenzburger, D.; Ellis, D. E. *Phys. Rev. B* **1980**, *22*, 4203.
(12) Sano, M.; Adachi, H.; Yamatera, H. *Bull. Chem. Soc. Jpn.* **1982**, *55*, 1022.
(13) Bowmaker, G. A.; Boyd, P. D. W.; Sorrensen, R. J. *J. Chem. Soc., Faraday Trans. 2* **1985**, *81*, 1627.
(14) Bancroft, G. M.; Chan, T.; Puddephatt, R. J.; Tse, J. S. *Inorg. Chem.* **1982**, *21*, 2946.
(15) DeKock, R. L.; Baerends, E. J.; Boerrigter, P. M.; Hengelmolen, R. *J. Am. Chem. Soc.* **1984**, *106*, 3387.
(16) (a) Mason, W. R. *J. Am. Chem. Soc.* **1973**, *95*, 3573. (b) Mason, W. R. *J. Am. Chem. Soc.* **1976**, *98*, 5182. (c) Koutek, M. E.; Mason, W. R. *Inorg. Chem.* **1980**, *19*, 648. (d) Chastian, S. K.; Mason, W. R. *Inorg. Chem.* **1982**, *21*, 3717.
(17) Janiak, C.; Hoffmann, R. *Inorg. Chem.* **1989**, *28*, 2743.

0020-1669/90/1329-3593$02.50/0

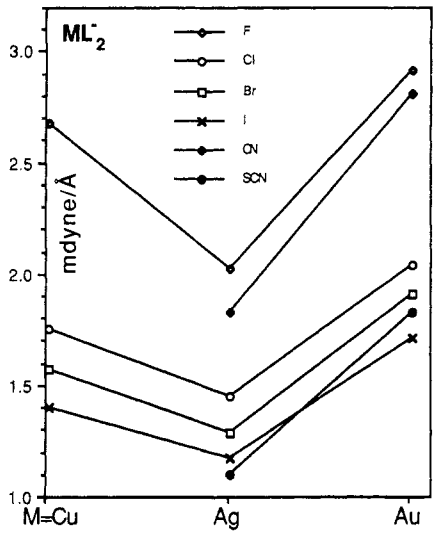

Figure 1. Experimental force constants for the ML_2^- complexes (M = Cu, Ag, Au; L = F, Cl, Br, I, CN, SCN) in mdyn/Å.[1] The M–F stretching force constants are derived from the CISC calculations (Table I), scaled by the factor given in Table IX. The M–S stretching force constants are estimated from the frequencies given in ref 3 and Table X.

Table I. Molecular Properties for the Linear Gold(I) Complexes AuL_2^- (L = H, CH_3, CN, PH_3^+, SCN, F, Cl, Br, I)[a]

ligand	method	r_e	k_e	D_e	D_e^1	D_e^2	ΔD_e^{12}
H	NR	1.902	0.928	297.5	187.0	110.5	76.5
	R	1.706	1.752	358.1	248.7	109.4	139.3
CH_3	NR	2.375	0.890	106.1	103.2	2.9	100.3
	R	2.190	1.782	174.1	126.9	47.2	79.7
CN	NR	2.322	1.001	512.3	251.3	261.0	−9.7
	R	2.075	2.246	595.6	352.5	243.1	109.4
SCN	NR	2.706	0.642	321.7	182.9	138.8	44.1
	R	2.430	1.207	333.2	239.5	95.0	144.5
SCN[b]	NR	2.759	0.524	199.0	145.3	53.7	91.6
	R	2.537	0.677	84.8	154.6	−69.8	224.4
PH_3	NR	2.793	0.430	204.6	98.5	106.1	−7.6
	R	2.453	1.047	378.4	196.8	181.6	15.2
F	NR	2.236	1.196	410.7	247.6	163.1	84.5
	R	2.017	2.253	406.9	318.3	88.6	229.7
	R/CI	2.028	2.396	483.2	316.5	166.7	149.8
	R/CISC	2.032	2.387	600.8	385.3	215.5	169.8
Cl	NR	2.630	0.781	428.0	210.1	217.9	−7.8
	R	2.398	1.458	416.1	255.4	160.7	94.7
	R/CI	2.358	1.631	395.5	234.8	176.8	58.0
	R/CISC	2.353	1.670	509.8	289.1	220.7	68.4
Br	NR	2.750	0.829	403.0	200.3	202.7	−2.4
	R	2.526	1.466	382.2	228.1	157.2	74.0
	R/CI	2.488	1.556	412.1	222.8	189.3	33.5
	R/CISC	2.487	1.585	501.7	276.8	224.9	51.9
I	NR	2.934	0.700	371.8	180.4	191.4	−11.0
	R	2.710	1.168	347.1	194.7	152.4	69.3
	R/CI	2.669	1.349	387.4	215.6	171.8	43.8
	R/CISC	2.668	1.373	474.1	267.9	206.2	61.7

[a] Au–X bond distance r_e in Å, dissociation energy $D_e(AuL_2^- \rightarrow Au + L + L^-)$ in kJ/mol, and force constant k_e for the symmetric stretching in mdyn/Å. See also Table III for additional calculated properties. D_e^1: dissociation energy for $AuL_2^- \rightarrow AuL + L^-$. D_e^2: dissociation energy for $AuL \rightarrow Au + L$. $D_e = D_e^1 + D_e^2$. $\Delta D_e^{12} = D_e^1 - D_e^2$. AuH_2^- dissociates into $AuH^- + H$; hence, we have chosen D_e^1 for $AuH_2^- \rightarrow AuH^- + H$ and D_e^2 for $AuH^- \rightarrow Au^- + H$. D_e^1 and D_e^2 for $Au(PH_3)_2^+$ are defined as $Au(PH_3)_2^+ \rightarrow AuPH_3^+ + PH_3 \rightarrow Au^+ + 2PH_3$. [b] Au—S—C≡N structure constrained to be linear.

hyperfine effects including spin–orbit coupling in AuF_2^-, $AuCl_2^-$, and $Au(CN)_2^-$ using the discrete variational Xα method (DVMXα).[11] The same method was used by Sano et al. to study the bonding and photoelectron spectra of the silver and gold cyano complexes.[12] Bowmaker and Boyd et al. studied nuclear quadrupole coupling on several AuL_2^- species (L = Cl, Br, I, CN) by using a nonrelativistic multiple-scattering Xα method (MSXα).[13] These authors found an unusually large ^{35}Cl nuclear quadrupole coupling constant (NQCC) in $AuCl_2^-$ compared to $CuCl_2^-$, which will be investigated in this paper. Bancroft et al. studied the ligand field splitting and Au(5d) participation in $AuCH_3(P(CH_3)_3)$ within the MSXα approximation.[14] The bonding and 5d participation in this compound have also been studied by DeKock et al. using a HF–Slater method (HFS).[15] Mason and co-workers studied ligand to metal charge-transfer transitions (LMCT) on several Au(I) complexes.[16] Janiak and Hoffmann recently studied linear halogen-bridged gold chains using the extended Hückel tight-binding method.[17] Ab initio calculations on linear Au(I) complexes have not so far been published.[9]

In this paper, we study in detail the relativistic effects in linear two-coordinated AuL_2^- complexes (L = H, F, Cl, Br, I, CN, SCN,

Table II. Optimized HF Geometries of the AuL and AuL_2^- Species (for the Au–L Bond Distances, See Table I)[a]

molecule	bond or angle
$AuCH_3$	C–H, 1.085 (1.083); Au–C–H, 109.2 (108.3)
$Au(CH_3)_2^-$	C–H, 1.095 (1.095); Au–C–H, 111.6 (111.8)
CH_3/CH_3^-	C–H, 1.075/1.098; H–C–H, 120.0/109.8
AuCN	C–N, 1.143 (1.138)
$Au(CN)_2^-$	C–N, 1.147 (1.144)
CN/CN^-	C–N, 1.157/1.157
$AuPH_3$	P–H, 1.419 (1.419); Au–P–H, 122.0 (121.9); H–P–H, 94.6 (94.7)
$AuPH_3^+$	P–H, 1.407 (1.401); Au–P–H, 117.9 (115.3)
$Au(PH_3)_2^+$	P–H, 1.407 (1.403); Au–P–H, 118.2 (116.3)
PH_3/PH_3^+	P–H, 1.421/1.400; H–P–H, 94.0/112.5
AuSCN	S–C, 1.702 (1.705); C–N, 1.143 (1.140); Au–S–C, 94.0 (99.1)
AuSCN[b]	S–C, 1.672 (1.670); C–N, 1.140 (1.141)
$Au(SCN)_2^-$	S–C, 1.695 (1.700); C–N, 1.142 (1.140); Au–S–C, 101.7 (102.6)
$Au(SCN)_2^{-b}$	S–C, 1.675 (1.668); C–N, 1.142 (1.142)
SCN/SCN^-	S–C, 1.648/1.686; C–N, 1.161/1.150

[a] Distances r_e in Å, angles α in degrees. Relativistic values are given in brackets. [b] Au—S—C≡N structure constrained to be linear.

Table III. Molecular Properties for the AuL Compounds (L = CH_3, CN, PH_3^+, SCN) at the HF Level[a]

molecule	method	r_e	k_e	D_e	μ_e
$AuCH_3$	NR	2.322	1.242	2.9	4.535
	R	2.017	1.879	47.2	2.218
AuCN	NR	2.297	1.278	261.0	10.585
	R	2.026	2.355	243.1	8.147
$AuPH_3$	NR	4.173	0.008	5.8	2.388
	R	4.240	0.008	8.3	1.328
$AuPH_3^+$	NR	2.825	0.725	106.1	
	R	2.429	0.997	196.8	
AuSCN	NR	2.648	0.913	138.8	10.483
	R	2.382	1.541	95.0	7.643
AuSCN[b]	NR	2.629	0.767	53.7	14.585
	R	2.434	1.318	−69.8	12.613

[a] Au–L bond distance r_e in Å, dissociation energy $D_e(AuL \rightarrow Au + L)$ in kJ mol^{-1}, force constant k_e in mdyn/Å, and dipole moment μ_e in D. See also Table III for additional calculated properties and ref 2. [b] Au—S—C≡N structure constrained to be linear.

Table IV. Relativistic HF Contributions in Au(I) Compounds per Au–L bond[a]

molecule	$\Delta_R r_e$	$\Delta_R D_e$	$\Delta_R k_e$
AuH_2^-	0.196	−30.3	−0.824
$Au(CN)_2^-$	0.245	−38.7	−1.245
$Au(SCN)_2^-$	0.276	−5.8	−0.565
$Au(SCN)_2^{-b}$	0.222	57.1	−0.153
$Au(CH_3)_2^-$	0.185	−34.0	−0.892
$Au(PH_3)_2^+$	0.340	−86.9	−0.617
AuF_2^-	0.219	1.9	−1.057
$AuCl_2^-$	0.232	11.9	−0.677
$AuBr_2^-$	0.224	20.8	−0.637
AuI_2^-	0.224	24.7	−0.468

[a] Distances r_e in Å, dissociation energies D_e in kJ/mol, and force constant k_e in mdyn/Å. [b] Au—S—C≡N structure constrained to be linear.

Table V. Mulliken Population Analysis for the Au(I) Compounds at the HF Level[a] Including Gross Atomic Orbital Populations n and Total Charges q ($q = 11 - n_{6s} - n_{5d} - n_{6p}$) for the Au Atom

	NR				R			
molecule	n_{6s}	n_{5d}	n_{6p}	q	n_{6s}	n_{5d}	n_{6p}	q
AuH	0.49	9.96	0.07	0.48	0.91	9.80	0.02	0.27
AuH_2^-	0.46	9.88	0.21	0.45	1.66	9.77	0.29	−0.72
$AuCH_3$	0.54	9.96	0.07	0.43	0.90	9.86	0.08	0.16
$Au(CH_3)_2^-$	0.53	9.88	0.16	0.43	0.97	9.76	0.19	0.08
AuCN	0.23	9.96	0.08	0.73	0.89	9.81	0.11	0.20
$Au(CN)_2^-$	0.56	9.87	0.06	0.51	1.80	9.65	0.24	−0.70
$AuPH_3^+$	0.18	9.97	0.09	0.76	0.49	9.88	0.09	0.54
$Au(PH_3)_2^+$	0.34	9.89	0.17	0.59	0.83	9.77	0.19	0.21
AuSCN	0.29	10.0	0.13	0.57	0.81	9.92	0.17	0.10
AuSCN[a]	0.07	10.0	0.10	0.82	0.27	9.96	0.14	0.63
$Au(SCN)_2^-$	0.34	9.98	0.18	0.49	1.06	9.82	0.33	−0.21
$Au(SCN)_2^-$[a]	0.12	10.0	0.09	0.79	0.39	9.88	0.29	0.44
AuF	0.10	9.99	0.07	0.82	0.33	9.92	0.10	0.65
AuF_2^-	0.23	9.98	0.08	0.71	0.80	9.67	0.15	0.37
AuCl	0.22	10.01	0.13	0.64	0.38	10.03	0.14	0.45
$AuCl_2^-$	0.27	9.98	0.17	0.57	0.93	9.78	0.24	0.05
AuBr	0.28	10.01	0.16	0.55	0.41	10.04	0.14	0.42
$AuBr_2^-$	0.25	9.99	0.23	0.52	0.94	9.80	0.27	−0.01
AuI	0.66	9.97	0.19	0.18	0.44	10.09	0.14	0.32
AuI_2^-	0.31	9.97	0.22	0.51	0.95	9.86	0.33	−0.14

[a] Au—S—C≡N structure constrained to be linear.

Table VI. Crystal Data Collection and Refinement Data for $[Ph_4As][Au(SCN)_2]$

chem formula	$AsAuC_{26}H_{20}N_2S_2$
cryst system	monoclinic
space group	$C2/c$
mol wt	698.175
a, Å	16.758 (3)
b, Å	7.183 (1)
c, Å	22.160 (4)
β, deg	111.92 (1)
Z	4
V, Å^3	2474.6 (6)
μ, cm^{-1}	73.06
ρ(calcd), g cm^{-3}	1.874
radiation	Mo Kα (0.71073 Å)
temp, K	173
no. of data collcd	2109
no. of unique reflcns ($F_o^2 > 3\sigma(F_3^2)$)	1177
F(000)	1336
no. of params	150
R, R_w	0.037, 0.041

CH_3), as well as in $Au(PH_3)_2^+$, $AuPH_3$, $AuPH_3^+$, $AuCH_3$, AuCN, and AuSCN, using multielectron adjusted nonrelativistic and relativistic spin–orbit averaged pseudopotentials within the Hartree–Fock (HF) approach. Configuration interaction (CI) calculations with single and double substitutions have been performed for the gold halide complexes. To support our computational results for $Au(SCN)_2^-$, we have synthesized $[AsPh_4][Au(SCN)_2]$ and examined this compound by infrared and Raman spectroscopy as well as by a single-crystal X-ray structure analysis. The results are presented in Tables I–XI and Figures 1–10 and will be discussed in the next section. The experimental and computational details are given in section III. A summary is given in section IV.

II. Results and Discussion

A. Geometries. During recent years, many structural studies on two-coordinate Au(I) compounds have been carried out. They have been reviewed by Melnik and Parish.[1] In all cases, a linear L–Au–L arrangement is preferred. Small deviations from 180° have been found only as a result of packing effects in the crystal or due to a weak interaction with a third ligand.[1] For the gold(I) halide complexes, our calculations confirm that in all cases the equilibrium geometry is the linear.[18–20] The measured gold–ligand bond distances from solid-state X-ray diffraction agree well with our calculated bond lengths, Table I–III. For example, the reported Au–C bond distance in $Au(CN)_2^-$ varies between 1.98 and 2.12 Å[21,22] (calculated 2.08 Å), and the C–N distance given by Jones et al.[22] is 1.16 Å (calculated 1.14 Å). Our relativistic CI bond lengths for the gold halide complexes are slightly overestimated by about 0.07–0.14 Å compared with the crystallographic data. For example, the Au–Cl bond distance is about 2.28 Å[23] (at the CI level 2.35 Å), the experimental Au–Br bond length in $AuBr_2^-$ is 2.40 Å[24] (CI 2.49 Å), and the Au–I bond distance given

Table VII

(a) Atom Coordinates (×10^4), Standard Deviations and Temperature Factors (Å^2 × 10^4) for $[Ph_4As][Au(SCN)_2]$

atom	x	y	z	U[a]
Au	0	0	0	37 (1)
S(1)	1312 (2)	833 (4)	−19 (2)	53 (1)
C(1)	1603 (6)	2531 (15)	545 (5)	35 (4)
N(1)	1833 (6)	3707 (2)	910 (5)	49 (4)
As	0	210 (2)	2500	21 (1)
C(11)	1257 (6)	−2653 (12)	2883 (5)	29 (4)
C(12)	1825 (6)	−3936 (12)	2794 (5)	30 (4)
C(13)	1957 (6)	−3984 (12)	2214 (5)	28 (4)
C(14)	1514 (6)	−2761 (13)	1723 (5)	32 (4)
C(15)	957 (5)	−1436 (13)	1804 (5)	28 (4)
C(16)	835 (5)	−1407 (12)	2387 (4)	21 (3)
C(21)	1400 (6)	1631 (13)	3602 (4)	29 (4)
C(22)	1758 (7)	2808 (14)	4128 (5)	37 (4)
C(23)	1263 (7)	4014 (14)	4317 (5)	41 (5)
C(24)	383 (8)	4108 (4)	3963 (6)	48 (5)
C(25)	9 (6)	2952 (13)	3425 (5)	32 (4)
C(26)	524 (5)	1762 (12)	3244 (4)	22 (3)
H(11)	1156	−2614	3277	39 (8)
H(12)	2120	−4804	3126	39 (8)
H(13)	2363	−4842	2156	39 (8)
H(14)	1591	−2844	1320	39 (8)
H(15)	668	−561	1473	39 (8)
H(21)	1745	743	3485	39 (8)
H(22)	2366	2773	4358	39 (8)
H(23)	1516	4785	4688	39 (8)
H(24)	29	4955	4088	39 (8)
H(25)	−597	2987	3186	39 (8)

(b) Anisotropic Temperature Factors (Å^2 × 10^4) and Standard Deviations for $[Ph_4As][Au(SCN)_2]$

atom	U_{11}	U_{22}	U_{33}	U_{23}	U_{13}	U_{12}
Au	45 (1)	24 (1)	27 (1)	−3 (1)	−6 (1)	2 (1)
S(1)	59 (2)	38 (1)	54 (2)	−23 (2)	13 (2)	−2 (1)
C(1)	37 (6)	39 (6)	24 (5)	−3 (5)	3 (5)	2 (5)
N(1)	47 (6)	55 (6)	41 (6)	−10 (5)	11 (5)	−13 (5)
As	23 (1)	18 (1)	19 (1)	−1 (4)	4 (1)	−18 (3)
C(11)	32 (5)	26 (5)	30 (6)	−4 (5)	15 (5)	−6 (4)
C(12)	22 (5)	20 (5)	44 (6)	5 (5)	7 (5)	7 (4)
C(13)	23 (5)	24 (5)	41 (6)	−4 (5)	15 (5)	−3 (4)
C(14)	39 (6)	29 (6)	31 (6)	−9 (5)	16 (5)	−6 (5)
C(15)	22 (5)	34 (5)	27 (5)	−2 (5)	5 (4)	−3 (4)
C(16)	5 (4)	32 (5)	20 (5)	1 (4)	−2 (4)	1 (4)
C(21)	36 (6)	23 (5)	27 (5)	6 (4)	11 (5)	0 (4)
C(22)	44 (6)	37 (6)	19 (5)	−4 (5)	−0 (5)	−8 (5)
C(23)	77 (9)	26 (5)	18 (5)	−6 (5)	14 (6)	−6 (5)
C(24)	61 (8)	33 (5)	41 (7)	−8 (6)	8 (6)	14 (6)
C(25)	24 (5)	31 (5)	33 (6)	−7 (5)	−0 (4)	6 (4)
C(26)	22 (5)	18 (4)	23 (5)	−3 (4)	6 (4)	−1 (4)

[a] Equivalent isotropic U defined as one-third of the trace of the orthogonalized U tensor.

(18) This may be seen as trivial, but CaF_2 for example is known for its bent geometry in gas phase,[19] probably due to polarization effects.[20]

(19) Büchler, A.; Stauffer, J. L.; Klemperer, W. *J. Chem. Phys.* **1964**, *40*, 3471.
(20) Szentpály, L. v.; Schwerdtfeger, P. *Chem. Phys. Lett.*, in press.
(21) Rosenzweig, A.; Cromer, D. T. *Acta Crystallogr.* **1959**, *12*, 709.
(22) Jones, P. G.; Clegg, W.; Sheldrick, G. M. *Acta Crystallogr.* **1977**, *B33*, 137.
(23) Berthold, H. J.; Ludwig, W. *Z. Naturforsch., B* **1980**, *35*, 970.
(24) Strähle, J.; Gelinek, J.; Kölmel, M.; Nemecek, A. M. *Z. Anorg. Allg. Chem.* **1979**, *456*, 241.

Table VIII. Interatomic Distances (Å) and Bond Angles (deg) for $[Ph_4As][Au(SCN)_2]$

Bond Distances			
Au-S(1)	2.295 (4)	C(13)-C(14)	1.394 (13)
S(1)-C(1)	1.697 (11)	C(14)-C(15)	1.392 (15)
C(1)-N(1)	1.142 (14)	C(15)-C(16)	1.397 (15)
As-C(16)	1.905 (9)	C(21)-C(26)	1.398 (12)
As-C(26)	1.934 (9)	C(22)-C(23)	1.369 (17)
C(11)-C(12)	1.388 (14)	C(23)-C(24)	1.400 (16)
C(11)-C(16)	1.406 (12)	C(24)-C(25)	1.412 (15)
C(12)-C(13)	1.400 (17)	C(25)-C(26)	1.376 (15)
		C(21)-C(22)	1.398 (13)

Bond Angles			
S(1)-Au-S(1)′	180.0 (1)	C(11)-C(12)-C(13)	120.0 (9)
Au-S(1)-C(1)	100.9 (4)	C(12)-C(13)-C(14)	120.1 (9)
S(1)-C(1)-N(1)	175.9 (12)	C(13)-C(14)-C(15)	121.1 (11)
C(16)-As-C(26)	110.0 (4)	C(14)-C(15)-C(16)	118.0 (8)
C(16)-As-C(16)′	110.0 (4)	C(11)-C(16)-C(15)	122.0 (9)
C(26)-As-C(26)′	110.0 (4)	C(22)-C(11)-C(26)	118.9 (10)
As-C(16)-C(11)	117.8 (8)	C(21)-C(22)-C(23)	121.5 (9)
As-C(16)-C(15)	120.0 (6)	C(22)-C(23)-C(24)	119.1 (9)
As-C(26)-C(21)	120.7 (7)	C(23)-C(24)-C(25)	120.4 (1)
As-C(26)-C(25)	118.5 (6)	C(24)-C(25)-C(26)	119.2 (9)
C(12)-C(11)-C(16)	118.8 (10)	C(21)-C(26)-C(25)	120.8 (8)

Table IX. CI Vibrational Frequencies in ω (cm^{-1}) and Force Constants k (mdyn/Å) for Gold Halide Complexes[a]

L	method	ω(I)	ω(II)	ω(III)	k_r	k_α	f_s
F	CI	462	504	157	2.387	0.115	
	scaled[b]	520	545	190	2.91	0.12	1.22
Cl	CI	283	330	93	1.670	0.067	
	exptl	329	350	116	2.04	0.102	1.22
Br	CI	183	247	68	1.585	0.060	
	exptl	209	254	77	1.91	0.081	1.21
I	CI	136	205	50	1.373	0.041	
	exptl	158	210	63	1.71	0.061	1.25

[a] (I) symmetric L-Au-L stretching mode; (II) asymmetric L-Au-L stretching mode; (III) L-Au-L bending mode. Experimental values from ref 2. k_r is the Au-L stretching force constant; k_α is the L-Au-L bending force constant (bond-bond interaction force constants have been neglected; see text). [b] Off-diagonal force-constant $k_{rr'}$ = 0.12 mdyn/Å assumed.[1]

recently by Wang et al.[25] is 2.53 Å (CI 2.67 Å). This may be due to differences between the gaseous and solid-state structures and to the approximations used in our calculations. The Au-C bond length in $Au(CH_3)(P(C_6H_5)_3)$ is about 2.12 Å[26] (the calculated value for $Au(CH_3)_2^-$ is 2.19 Å). The calculated Au-P bond length for $Au(PH_3)_2^+$ (2.45 Å) is 0.16 Å larger than the experimentally given Au-P bond distance in $Au(PPh_3)_2^+$ (2.29 Å;[1] Ph = C_6H_5). While CI treatment would probably lead to a shorter Au-P bond length, the electron-withdrawing phenyl groups can also be expected to cause a shortening in the Au-P bond distance compared with the H atom. Direct comparison with our calculated values may, therefore, not be appropriate. The importance of using polarization functions for the P atom becomes quite significant for the Au-P bond in $Au(PH_3)_2^+$. Using only a 6-311G basis set (without d functions) for the P atom, we obtained a Au-P bond distance of 2.489 Å, i.e. about 0.4 Å larger than the r_e value obtained with the 6-311G* basis set.

All gold complexes show relativistic bond contractions $\Delta_R r_e = r_e^{NR} - r_e^R$ between 0.19 and 0.34 Å, calculated at the HF level (Table IV). This contraction can also be observed in the few known bond lengths available from the literature,[24,27] e.g., $CuBr_2^-$, 2.22 Å; $AgBr_2^-$, 2.45 Å; and $AuBr_2^-$, 2.49 Å (compared with the calculated nonrelativistic bond distance of $AuBr_2^-$, 2.75 Å). Hence, the unexpected trend in the group 11 bond lengths is caused by relativistic effects and is similar to that obtained earlier for the diatomic compounds, as discussed and analyzed in detail in ref 7. Ahrland et al. have recently studied the thermodynamics of the formation of the group 11 halide and thiocyanate complexes in pyridine and acetonitrile[28] and have estimated gold–solvent bond distances by means of the EXAFS technique. The same trends were evident (for example, in acetonitrile the metal–nitrogen bond distances are 1.99 Å for Cu, 2.25 Å for Ag, and 2.19 Å for Au[28]).

Table X. Experimental and Calculated Wavenumbers ω (cm^{-1}) and Adjusted Harmonic Valence Force Field k (Diagonal k_d and Nondiagonal k_n Force Constants in mdyn/Å of Vibrational Bands of $Au(SCN)_2^-$[a]

	IR		Raman			
mode	exptl	calc	exptl	calc	k_d	k_n
C-N str	2120	2120	2118	2118	15.655	−0.010
S-C str	(699)[b]	699	695	695	4.424	−0.016
S-C-N bend	(454)[b]	454	450	452	0.168	−0.005
Au-S str	310	310	306	305	1.828	0.275
Au-S-C bend	144	144	108	111	0.226	0.001
S-Au-S bend	110	93			0.233	

[a] The point group C_{2h} has been used (A_g (Raman active); B_u (IR active)). The observed 100-cm^{-1} line is a A_g rotatory R_z mode. ϵ = 18 cm^{-1} (eq 2). [b] Assumed (masked by Ph_4As^+).

Additional structural information about these compounds is listed in Table II, together with data for the ligands where appropriate, at both the nonrelativistic and relativistic levels of the theory. Atoms not directly bound to the Au atom show very small relativistic bond contractions (<0.04 Å), which are negligible compared with the errors produced by the algebraic HF or the pseudopotential approximation for gold. Table V shows the Mulliken population analysis of the Au(I) complexes compared with that of the singly bonded gold compounds. The AuL_2^- species show larger 5d and 6p contributions than do the AuL compounds. This additional metal–ligand overlap should shorten the Au-L bond. In contrast to this prediction, however, a comparison of the bond distances for the two species AuL and AuL_2^- (Tables I and III and ref 7) shows in all cases that $r_e^R(AuL_2^-) > r_e^R(AuL)$. One reason for this bond lengthening may be the additional negative charge in the AuL_2^- compounds, which increases the Au(6s) population (Table V). This leads to a more diffuse Au(6s) orbital, as shown by the comparison of the $\langle r \rangle$ expectation values (in au) of the 6s orbital in Au^+ ($5d^96s^1$; $J = 2$) with Au and Au^-, $\langle r \rangle_{Au^+} = 2.68$, $\langle r \rangle_{Au} = 3.06$, and $\langle r \rangle_{Au^-} = 3.77$,[29] and we expect that a more diffuse Au(6s) orbital should lead to larger gold–ligand bond distances. Similar effects have been found in copper fluorides with $r_e^R(CuF_2^-) > r_e^R(CuF) > r_e^R(CuF_2)$.[30] The maximum relativistic change in bond angle, $\Delta_R\alpha = \alpha_{NR} - \alpha_R$, is −5.1° found for the Au-S-C angle in the AuSCN molecule. This value is large when compared to previously published relativistic bond angle changes; for example in PbH_2, $\Delta_R\alpha$(H-Pb-H) = 0.9°.[31]

The Molecular Structure of $Au(SCN)_2^-$. It is surprising that the structures of AuSCN or of $Au(SCN)_2^-$ have not been previously determined.[32] The crystal structure of $Au(SCN)(PPh_3)_2$ shows the normal bent Au-S-C conformation with an angle of 107.6°.[33] However, ionic bonding between the metal center and the thiocyanate ligand (M^+SCN^-) could lead to a linear Au-S-C

(25) Wang, H. H.; Montgomery, L. K.; Geiser, U.; Porter, L. C.; Carlson, K. D.; Ferraro, J. R.; Williams, J. M.; Cariss, C. S.; Rubinstein, R. L.; Whitworth, J. R.; Evain, M.; Novoa, J. J.; Whangbo, M. H. *Chem. Mater.* **1989**, *1*, 140.
(26) Gavens, P. D.; Guy, J. J.; Mays, M. J.; Sheldrick, G. M. *Acta Crystallogr.* **1980**, *B36*, 160.
(27) (a) Hathaway, B. J. In *Comprehensive Coordination Chemistry*; Pergamon: Oxford, England, 1987; Vol. 5, p 533. (b) Lancashire, R. J. In *Comprehensive Coordination Chemistry*; Pergamon: Oxford, England, 1987; Vol. 5, p 775.
(28) Ahrland, S.; Nilssen, K.; Persson, I.; Yuchi, A.; Penner-Hahn, J. E. *Inorg. Chem.* **1989**, *28*, 1833.
(29) Grant, I. P.; McKenzie, B. J.; Norrington, P. H.; Mayers, D. F.; Pyper, N. C. *Comput. Phys. Commun.* **1980**, *21*, 207.
(30) Schwerdtfeger, P.; Aldridge, L. P.; Boyd, P. D. W.; Bowmaker, G. A. *Struct. Chem.*, in press.
(31) (a) Schwerdtfeger, P.; Silberbach, H.; Miehlich, B. *J. Chem. Phys.* **1989**, *90*, 762. (b) Hafner, P.; Habitz, P.; Ishikawa, Y.; Wechsel-Trakowski, E.; Schwarz, W. H. E. *Chem. Phys. Lett.* **1981**, *80*, 311.
(32) Norbury, A. H. *Adv. Inorg. Chem.* **1975**, *17*, 232.
(33) Muir, J. A.; Muir, M. M.; Arias, S. *Acta Crystallogr.* **1982**, *B38*, 1318, 2047.

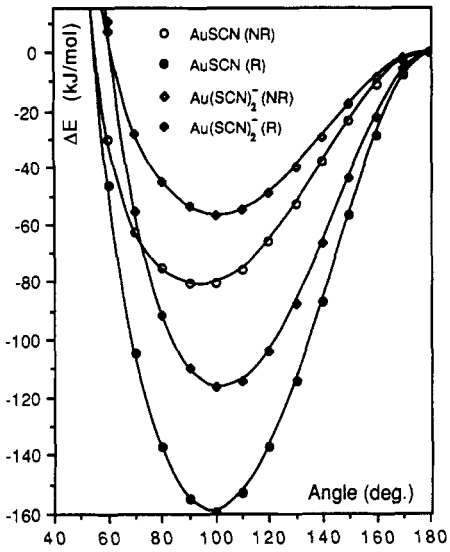

Figure 2. HF potential curve $\Delta E(\gamma)$ per Au–S bond for the Au–S–C bending in AuSCN and $Au(SCN)_2^-$ (C_{2h}). The bond distances are taken from the linear compound (Tables I–III).

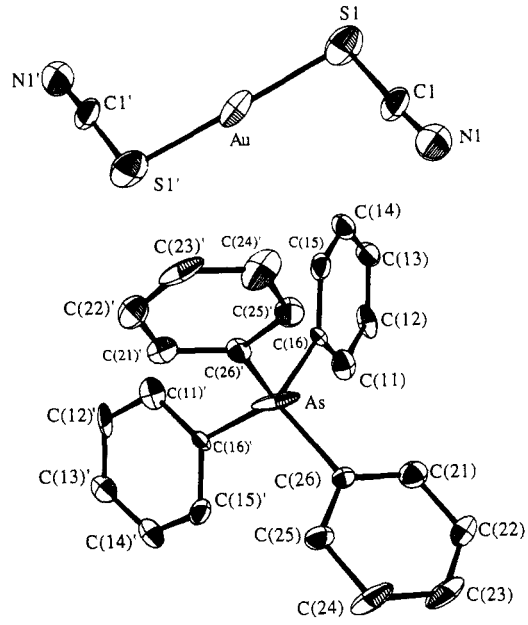

Figure 3. ORTEP representation of the X-ray crystal structure of the molecule $[AsPh_4][Au(SCN)_2]$.

arrangement due to crystal forces. Rogers discussed also the possibility of a linear covalent Au–S–C conformation.[3] The dependence of the total energy of AuSCN and $Au(SCN)_2^-$ on the Au–S–C angle is shown in Figure 2. The calculations clearly favor the bent conformation for both compounds, AuSCN and $Au(SCN)_2^-$, indicating a large amount of covalency in the Au–S bond. The differences in energy between the linear and bent structures are rather large at the HF level, e.g. more than 120 kJ/mol per Au–S bond in $Au(SCN)_2^-$.

To test the results of our calculations, we determined the solid state structure of $Au(SCN)_2^-$ in the compound $[AsPh_4][Au(SCN)_2]$ by a single-crystal X-ray diffraction (see section III for experimental details and Table VI). The structure of $[AsPh_4][Au(SCN)_2]$ consists of well-separated $Au(SCN)_2^-$ anions, each with gold atoms on crystallographic centers of inversion, and tetraphenylarsonium cations with each As atom located on a crystallographic 2-fold rotation axis. This results in a monoclinic unit cell of space group $C2/c$, Table VI. The coordinates of the 17 independent non-hydrogen atoms are listed in Table VII together with the calculated positions for 10 hydrogen atoms. Anisotropic thermal parameters for the non-hydrogen atoms are listed in Table VIII. An ORTEP representation (50% probability level) of $[AsPh_4][Au(SCN)_2]$ is given in Figure 3. The hydrogen atoms have been omitted for clarity.

The measured Au–S bond distance of 2.295 Å (Table VIII) is relatively short compared with our calculated HF value of 2.430 Å (Table I) or with the crystallographic value of 2.468 Å in $Au(SCN)(PPh_3)_2$.[33] Other calculated geometry parameters agree very well with the measured values; i.e., the C–N and S–C bond distances agree within 0.003 Å and the calculated HF Au–S–C bond angle differs only by 1.7° from experiment. This indicates that the electron correlation must be the included to obtain a shorter Au–S bond distance, as was the case also for the Au–P bond in $Au(PH_3)_2^+$. However, a CI procedure would be very time consuming for this compound (see, for example, the discussion in section III). We therefore included electron correlation by using a Møller–Plesset perturbation procedure (second order; MP2) and optimized the Au–S bond distance in $Au(SCN)_2^-$. At this level of approximation, we obtained a shorter bond distance of 2.362 Å for the Au–S bond relative to the HF value. This is in better agreement with the experimental value.

B. Force Constants. The CI frequencies for the halides are compared with the experimental values in Table IX. The force constants have been derived from the symmetric L–Au–L stretching mode; hence, the CI values should correspond to the symmetric force constants, $k_r + k_{rr'}$. In all cases, they agree reasonably with experiment. The best agreement is obtained for the iodo complex, AuI_2^-. Obviously, the more ionic the Au–L bond, the more difficult it is to obtain accurate force constants. A similar situation was found recently in CI calculations of the zinc monohalides.[34] A larger CI space, higher substitutions in the CI wave function, and more basis functions are therefore needed to obtain force constants in better agreement with experiment. However, CISD (see section III) systematically underestimates the experimentally based force constants, so it is possible to predict the AuF_2^- spectrum by a scaling procedure. The scaling factor $f_s = 1.22$ has been obtained from the deviations from the experimental values for the other halide complexes AuL_2^- (L = Cl, Br, I). The scaling factors are given in Table IX. Since the off-diagonal force constant $k_{rr'}$ is quite significant for predicting the correct separation of the symmetric/asymmetric stretching frequencies, we used a value of $k_{rr'} = 0.12$ mdyn/Å, which was also obtained by a fitting procedure using the values for the other halides.[2] The predicted frequencies for AuF_2^- are listed in Table IX. The relatively large force constant and CI dissociation energy (Table I) give clear evidence for the stability of this compound; hence, this species should be observable, at least in matrix isolation. As pointed out in the second paper of this series,[9] $M[AuF_2]$ is expected to be (chemically) stable as long as the counterion M^+ has a weak M–F bond to avoid the disproportionation

$$3MAuF_2 \rightarrow MAuF_4 + 2MF + 2Au \qquad (1)$$

We suggest that cations such as $[N(CH_3)_4]^+$ or $[AsPh_4]^+$ could be used for this purpose. Since even mixed-fluoride–halide species of the form $AuFL^-$ (L = Cl, Br, I) are unknown, we suggest as a first step in preparing a species containing a Au(I)–F bond the reaction of AuX (X = Cl, Br, I) with fluorides MF (M = $[N(CH_3)_4]$, $[AsPh_4]$, ...).

Figure 1 shows the experimentally known Au–L stretching force constants for some group 11 complexes. As discussed previously for the diatomic gold compounds,[7] the Au–L force constants decrease from copper to silver, but increase in all cases from silver to gold. The relativistic HF contributions of the force constants $\Delta_R k_e$ for the AuL_2^- complexes are listed in Table IV. These data clearly show that the trend is caused by relativistic effects as explained in detail for various diatomic gold compounds.[7] The calculated value of $\Delta_R k_e$ (Au–L) for $Au(CN)_2^-$ (ca. 1.25 mdyn/Å) and for AuCN (ca. 1.08 mdyn/Å) are very large. Figure 1 shows that this is also observed at the experimental level; i.e., the Au–C stretching force constants increase strongly from $Ag(CN)_2^-$ to $Au(CN)_2^-$. It can now be seen that this trend is a relativistic effect

(34) Bowmaker, G. A.; Schwerdtfeger, P. *J. Mol. Struct., THEOCHEM.* **1990**, *205*, 295.

Table XI. HF Valence Orbital Energies (in au) and Major Atomic Orbital Contributions for the Au(I) Complexes at the HF Equilibrium Distances (Table I)[a]

ligand	method	sym	orbital energy	contribns	method	sym	orbital energy	contribn
F	NR	σ_g	−0.234	Au(s,d); F(p)	R	σ_g	−0.194	Au(s,d); F(p) [F(s)]
		π_g	−0.275	Au(d); F(p)		π_g	−0.248	Au(d); F(p)
		σ_u	−0.303	F(p); Au(p) [F(s)]		δ_g	−0.283	Au(d)
		π_g	−0.305	F(p) [Au(p)]		σ_u	−0.338	F(p); Au(p) [F(s)]
		δ_g	−0.342	Au(d)		π_u	−0.352	F(p) [Au(p)]
		π_g	−0.358	Au(d); F(p)		π_g	−0.389	Au(d); F(p)
		σ_g	−0.387	Au(d); F(p) [Au(s); F(s)]		σ_g	−0.425	Au(s,d); F(p) [F(s)]
		σ_u	−1.192	F(s) [Au(p); F(p)]		σ_u	−1.246	F(s) [Au(p); F(p)]
		σ_g	−1.193	F(s) [Au(s,d); F(p)]		σ_g	−1.254	F(s) [Au(s,d); F(p)]
Cl	NR	π_g	−0.234	Cl(p); Au(d)	R	π_g	−0.227	Au(d); Cl(p)
		σ_g	−0.235	Au(s,d); Cl(p) [Cl(s)]		σ_g	−0.228	Au(s,d); Cl(s,p)
		π_u	−0.244	Cl(p) [Au(p)]		π_u	−0.261	Cl(p) [Au(p)]
		σ_u	−0.252	Cl(p); Au(p) [Cl(s)]		σ_u	−0.268	Cl(p); Au(p) [Cl(s)]
		δ_g	−0.385	Au(d)		δ_g	−0.312	Au(d)
		π_g	−0.387	Au(d) [Cl(p)]		π_g	−0.350	Au(d); Cl(p)
		σ_g	−0.398	Au(d); Cl(p) [Au(s); Cl(s)]		σ_g	−0.378	Au(d,s); Cl(p) [Cl(s)]
		σ_u	−0.831	Cl(s) [Au(p)]		σ_u	−0.850	Cl(s) [Au(p); Cl(p)]
		σ_g	−0.835	Cl(s) [Au(s,d)]		σ_g	−0.859	Cl(s) [Au(s,d); Cl(p)]
Br	NR	π_g	−0.218	Br(p); Au(d)	R	π_g	−0.211	Au(d); Br(p)
		π_u	−0.226	Br(p) [Au(p)]		σ_g	−0.231	Au(s,d); Br(s,p)
		σ_g	−0.229	Au(s,d); Br(p) [Br(s)]		π_u	−0.235	Br(p) [Au(p)]
		σ_u	−0.237	Br(p); Au(p) [Br(s)]		σ_u	−0.245	Br(p); Au(p) [Br(s)]
		δ_g	−0.395	Au(d)		δ_g	−0.321	Au(d)
		π_g	−0.396	Au(d) [Br(p)]		π_g	−0.348	Au(d); Br(p)
		σ_g	−0.404	Au(d); Br(p) [Au(s); Br(s)]		σ_g	−0.368	Au(d,s); Br(p) [Br(s)]
		σ_u	−0.778	Br(s) [Au(p)]		σ_u	−0.815	Br(s) [Au(p); Br(p)]
		σ_g	−0.782	Br(s) [Au(s,d); Br(p)]		σ_g	−0.823	Br(s) [Au(s,d); Br(p)]
I	NR	π_g	−0.198	I(p); Au(d)	R	π_g	−0.192	Au(d); I(p)
		π_u	−0.206	I(p) [Au(p)]		π_u	−0.210	I(p) [Au(p)]
		σ_u	−0.218	I(p); Au(p) [I(s)]		σ_u	−0.220	I(p,s); Au(p)
		σ_g	−0.219	Au(s,d); I(p) [I(s)]		σ_g	−0.231	Au(s,d); I(s,p)
		δ_g	−0.408	Au(d)		δ_g	−0.331	Au(d)
		π_g	−0.410	Au(d) [I(p)]		π_g	−0.353	Au(d) [I(p)]
		σ_g	−0.412	Au(d) [Au(s); I(s,p)]		σ_g	−0.364	Au(d,s); I(s,p)
		σ_u	−0.637	I(s) [Au(p); I(p)]		σ_u	−0.698	I(s); Au(p) [I(p)]
		σ_g	−0.643	I(s) [Au(s,d); I(p)]		σ_g	−0.708	I(s); Au(s) [Au(d); I(p)]
H	NR	σ_g	−0.135	Au(s,d); H(s)	R	σ_u	−0.142	H(s); Au(p)
		σ_u	−0.135	H(s); Au(p)		σ_g	−0.144	Au(s,d) [H(s)]
		π_g	−0.311	Au(d) [H(p)]		δ_g	−0.246	Au(d)
		δ_g	−0.315	Au(d)		π_g	−0.253	Au(d)
		σ_g	−0.341	Au(d) [Au(s); H(s)]		σ_g	−0.334	Au(d,s); H(s)
CH_3	NR	A_2''	−0.122	C(p,s); Au(p)	R	A_2''	−0.132	C(p,s); Au(p)
		A_1'	−0.125	Au(s,d); C(s,p) [H(s)]		A_1'	−0.134	Au(s,d); C(s,p) [H(s)]
		E''	−0.281	Au(d); C(s,p); H(s)		E''	−0.237	Au(d); C(p); H(s)
		E'	−0.306	Au(d) [C(p)]		E'	−0.252	Au(d) [C(p)]
		A_1'	−0.316	Au(d); C(p) [Au(s); H(s)]		A_1'	−0.303	Au(d); C(p) [Au(s); H(s)]
		E'	−0.328	C(p); H(s) [Au(p,d)]		E'	−0.336	C(p); H(s) [Au(p,d)]
		E''	−0.345	C(p); H(s); Au(d)		E''	−0.352	C(p); H(s); Au(d)
		A_2''	−0.697	C(s); H(s) [C(p); Au(p)]		A_2''	−0.702	C(s); H(s) [C(p); Au(p)]
		A_1'	−0.701	C(s); H(s) [C(p); Au(s,d)]		A_1'	−0.710	C(s); H(s) [C(p); Au(s,d)]
PH_3	NR	A_1'	−0.555	Au(s,d); P(s,p) [H(s)]	R	A_1'	−0.566	Au(s,d); P(s,p) [H(s)]
		A_2''	−0.571	P(p,s); Au(p) [H(s)]		A_2''	−0.594	P(p,s); Au(p) [H(s)]
		E''	−0.687	Au(d); P(p); H(s)		E''	−0.656	Au(d); [P(p); H(s)]
		E'	−0.696	Au(d)		E'	−0.659	Au(d); P(p) [H(s)]
		E'	−0.709	P(p); H(s)		E''	−0.724	P(p); H(s)
		E''	−0.717	Au(d); P(p); H(s)		E'	−0.735	Au(d); P(p); H(s)
		A_1'	−0.731	Au(d); P(p); [H(s); Au(s)]		A_1'	−0.741	Au(d,s); P(p) [H(s)]
		A_2''	−1.025	P(s); H(s) [P(p); Au(p)]		A_2''	−1.051	P(s); H(s) [P(p); Au(p)]
		A_1'	−1.027	P(s); H(s) [P(p); Au(s,d)]		A_1'	−1.058	P(s); H(s) [P(p); Au(s,d)]
CN	NR	σ_g	−0.265	Au(s,d); C(s,p); N(s,p)	R	σ_g	−0.252	Au(s,d); C(s,p); N(s,p)
		π_g	−0.281	Au(d); C(p); N(p)		π_g	−0.275	Au(d); C(p); N(p)
		π_u	−0.289	C(p); N(p) [Au(p)]		π_u	−0.304	C(p); N(p) [Au(p)]
		σ_u	−0.312	C(s,p); N(s,p); Au(p)		σ_u	−0.331	C(s,p); N(s,p); Au(p)
		σ_g	−0.389	C(s,p); N(s,p); Au(d) [Au(s)]		δ_g	−0.339	Au(d)
		δ_g	−0.392	Au(d)		π_g	−0.378	Au(d); C(p) [N(p)]
		π_g	−0.395	Au(d) [C(p); N(p)]		σ_g	−0.393	C(s,p); N(s,p); Au(s,d)
		σ_u	−0.435	C(s,p); N(s,p); Au(p)		σ_u	−0.450	N(s,p); C(s,p); Au(p)
		σ_g	−0.488	Au(s,d); C(s,p); N(s,p)		σ_g	−0.541	Au(s,d); C(s,p); N(s,p)
		σ_u	−1.028	C(s,p); N(s,p) [Au(p)]		σ_u	−1.042	C(s,p); N(s,p) [Au(p)]
		σ_g	−1.028	C(s,p); N(s,p); Au(s) [Au(d)]		σ_g	−1.042	C(s,p); N(s,p); Au(s) [Au(d)]

Table XI (Continued)

ligand	method	sym	orbital energy	contribns	method	sym	orbital energy	contribn
SCN ($D_{\infty h}$)	NR	π_g	−0.215	S(p); N(p); Au(d); C(p)	R	π_g	−0.215	S(p); N(p); Au(d); C(p)
		π_u	−0.221	S(p); N(p) [Au(p); C(p)]		π_u	−0.231	S(p); N(p) [Au(p); C(p)]
		π_g	−0.384	S(p); C(p); N(p); Au(d)		σ_g	−0.372	Au(s); S(s,p); C(s,p); N(s,p)
		π_u	−0.385	S(p); C(p); N(p)		π_g	−0.389	Au(d); S(p); C(p); N(p)
		σ_g	−0.401	Au(d,s); S(p,s); C(p,s); N(s,p)		π_u	−0.393	S(p); C(p); N(p) [Au(p)]
		σ_u	−0.413	S(p,s); C(p,s); N(s,p) [Au(p)]		δ_g	−0.417	Au(d)
		σ_g	−0.450	Au(d,s); S(s,p); C(s,p); N(s,p)		σ_u	−0.420	S(s,p); C(p,s); N(s,p) [Au(p)]
		δ_g	−0.482	Au(d)		σ_g	−0.434	Au(d,s); S(s,p); C(p,s); N(s,p)
		π_g	−0.485	Au(d) [S(p),C(p)]		π_g	−0.436	Au(d); S(p) [C(p),N(p)]
		σ_u	−0.497	S(s,p); C(s,p); N(s,p); Au(p)		σ_u	−0.508	Au(p); S(s,p); C(s,p); N(s,p)
		σ_g	−0.539	Au(d,s); S(p,s); C(s,p); N(s,p)		σ_g	−0.552	Au(s,d); S(p); C(s,p); N(s)
		σ_u	−0.853	S(s,p); C(s,p); N(s,p); Au(p)		σ_u	−0.865	S(s,p); C(s,p); N(s,p) [Au(p)]
		σ_g	−0.855	S(p); C(s,p); N(s,p); Au(s,d)		σ_g	−0.868	S(s,p); C(s,p); N(s,p) [Au(s,d)]
		σ_u	−1.117	Au(p); S(s,p); C(s,p); N(s,p)		σ_u	−1.124	Au(p); S(s,p); C(s,p); N(s,p)
		σ_g	−1.117	Au(s); S(s,p); C(s,p); N(s,p)		σ_g	−1.124	S(s,p); C(s,p); N(s,p) [Au(s,d)]
SCN (C_{2h})	NR	B_g	−0.216	S(p); N(p) [C(p),Au(d)]	R	B_g	−0.214	S(p); Au(d); N(p) [C(p)]
		A_u	−0.224	S(p); N(p) [C(p),Au(p)]		A_u	−0.237	S(p); N(p) [C(p); Au(p)]
		A_g	−0.229	Au(s,d); S(p,s); C(p,s); N(s,p)		B_u	−0.241	S(p,s); C(s,p); N(s,p); Au(p)
		B_u	−0.230	S(p,s); C(s,p); N(s,p); Au(p)		A_g	−0.245	Au(s,d); S(s,p); C(s,p); N(s,p)
		A_g	−0.377	Au(d,s); S(p,s); C(p,s); N(p,s)		A_g	−0.348	Au(d,s); S(s,p); C(s,p); N(s,p)
		B_g	−0.383	S(p); C(p); N(p); Au(d)		A_g	−0.353	Au(d,s); C(p,s); S(p,s); N(s,p)
		A_u	−0.386	S(p); C(p); N(p) [Au(p)]		B_g	−0.356	Au(d) [S(p); C(p); N(p)]
		B_u	−0.388	S(p,s); C(p,s); N(s,p) [Au(p)]		A_g	−0.359	Au(d,s); N(s,p); S(s,p); C(p,s)
		A_g	−0.397	Au(d,s); S(p,s); C(p,s); N(s,p)		B_g	−0.368	Au(d) [S(p); C(p); N(p)]
		B_u	−0.411	S(s,p); C(s,p); N(s,p) [Au(p)]		A_u	−0.393	S(p); C(p); N(p) [Au(p)]
		A_g	−0.429	Au(d,s); N(s,p); S(s,p); C(s,p)		B_u	−0.394	S(p,s); C(p,s); N(s,p) [Au(p)]
		B_g	−0.429	Au(d) [C(p); N(p)]		B_g	−0.407	Au(d); S(p); C(p); N(p)
		A_g	−0.431	Au(d) [C(s,p); N(s,p)]		B_u	−0.418	S(s,p); C(p,s); N(s,p) [Au(p)]
		B_g	−0.433	Au(d) [S(p); C(p); N(p)]		A_g	−0.419	Au(d,s); S(p,s); C(p,s); N(s,p)
		A_g	−0.440	Au(d); S(p,s); N(s,p); C(s,p)		A_g	−0.433	Au(d,s); S(p,s); C(p,s); N(s,p)
		B_u	−0.491	S(s,p); C(s,p); N(s,p) [Au(p)]		B_u	−0.502	S(s,p); C(s,p); N(s,p) [Au(p)]
		A_g	−0.507	S(s,p); C(s,p); N(s,p); Au(d,s)		A_g	−0.528	S(s,p); C(s,p); N(s,p); Au(d,s)
		B_u	−0.853	S(s,p); C(s,p); N(s,p) [Au(p)]		B_u	−0.865	S(s,p); C(s,p); N(s,p) [Au(p)]
		A_g	−0.855	S(s,p); C(s,p); N(s,p) [Au(s,d)]		A_g	−0.871	S(s,p); C(s,p); N(s,p) [Au(s,d)]
		B_u	−1.119	S(s,p); C(s,p); N(s,p) [Au(p)]		B_u	−1.126	S(s,p); C(s,p); N(s,p) [Au(p)]
		A_g	−1.119	S(s,p); C(s,p); N(s,p) [Au(s)]		A_g	−1.126	S(s,p); C(s,p); N(s,p) [Au(s)]

[a] Weak atomic orbital contributions (<10%) are set in brackets; very weak contributions (<2%) have been neglected. Point group symmetry is $D_{\infty h}$, except for $Au(CH_3)_2^-$ (D_{3h}) and nonlinear $Au(SCN)_2^-$ (C_{2h}).

and is not caused by $Au(d_\pi)$–$CN(\pi^*)$ bonding as suggested previously.[1a] As stated above, relativistic changes in intraligand bond lengths L_1–L_2 in gold compounds are very small and are negligible (Table II). The force constants, however, are more sensitive to small changes in electron densities. For $Au(CN)_2^-$, we calculated $\Delta_R k_e$ (C–N) ≈ −0.4 mdyn/Å at the HF level (compare with AuCN of $\Delta_R k_e$(C–N) ≈ −0.85 mdyn/Å), which is a change of only about 3% compared with the experimental k_e of 16.18 mdyn/Å.[35] This causes an increase in the C–N stretching frequency of about 25 cm^{-1}. To analyze these effects in more detail, we performed density plots for $Au(CN)_2^-$.

Figure 4 shows relativistic ρ_R and nonrelativistic ρ_{NR} as well as relativistic difference density plots $\Delta_R\rho = \rho_{NR} - \rho_R$ of $Au(CN)_2^-$. The binding σ_g and $2\pi_g$ orbitals as well as the nonbonding $1\pi_g$ orbital are presented, which describe the major bond contributions in this molecule. The sequence in orbital energies is $\epsilon(1\pi_g) > \epsilon(2\pi_g)$, and $1\pi_g$ denotes the HOMO of π_g symmetry and $2\pi_g$ denotes the next lowest occupied orbital of π_g symmetry. Similar MO contours for a series of orbitals have been published before by Sano et al.[35] for the molecule $Ag(CN)_2^-$. All density plots show the large Au(5d) contributions in the Au–CN bond. Relativistic difference densities $\Delta_R\rho$ describe charge flows due to relativistic effects. Dashed lines (negative areas) in $\Delta_R\rho$ in Figure 4 show sources (increase) and solid lines (positive areas) show sinks (decrease) of electron density. To understand the origin of such charge flows due to relativistic effects, we show the atomic radial densities and $\Delta_R\rho$ for the gold 6s and 5d orbitals in Figure 5. In regions $r > 1.7$ Å we obtain $\Delta_R\rho > 0$, corresponding to a loss in electron density, whereas in the region $0.6 < r < 1.7$ Å, $\Delta_R\rho < 0$, which corresponds to an increase in electron density due to the relativistic 6s contraction. In the region below 0.8 Å, we also have to consider the effects of the relativistic 5d expansion, which shows the reverse trend in sign of $\Delta_R\rho$(5d) relative to $\Delta_R\rho$(6s). Jones argued that an increase in the metal–ligand σ-bond strength increases that of the C–N bond.[35] The σ-HOMO of $Au(CN)_2^-$ (Figure 4A) shows an overall increase in electron density close to the $Au(CN)_2^-$ bond axis (caused by the relativistic 6s contraction, Figure 5) and also perpendicular to this direction at the Au center (caused by the relativistic 5d expansion, Figure 5). This increased density may explain the relativistically increased bond strength in both the Au–C and C–N bonds. Jones also argued that an increase in metal–ligand π-bonding decreases the C–N stretching frequency, and this can be seen in the series of C–N stretching force constants for the metal cyanide complexes of Ag, Au and Hg.[35] Both π orbitals show an increase in electron density in the C–N π bond, but a decrease in the Au–C π bond. This however cannot explain the trend in C–N stretching frequencies in the gold and silver compounds, i.e., $Ag(CN)_2^- > Au(CN)_2^-$. Further investigations are necessary to explain this behavior. A density plot of the σ_g and π_g orbitals of AuCN is shown in Figure 6. As in the case of $Au(CN)_2^-$, we see large Au(5d) contributions.

The force constants for the halide complexes of Au(I), AuL_2^-, are plotted together with those for the monohalides, AuL, in Figure 7. For all compounds, we find $k_e(AuL) > k_e(AuL_2^-)$. This trend has been observed previously for some copper and silver halides, for example in the series $k_e(CuBr) > k_e(CuBr_2^-) > k_e(CuBr_3^{2-})$.[2] It has been explained previously in terms of a progressive weakening of the metal–ligand bond from the neutral to the charged species.[2] From the energetic point of view, there is no weakening of the Au–L bond by adding another ligand L^- to AuL, i.e. $D_e^1 > D_e^2$ at the CI level for all halides (Table I). This causes the

(35) (a) Jones, L. H. *J. Chem. Phys.* **1965**, *43*, 594. (b) Jones, L. H. *Inorg. Chem.* **1963**, *2*, 777. (c) Chadwick, B. M.; Frankiss, S. G. *J. Mol. Struct.* **1976**, *31*, 1.

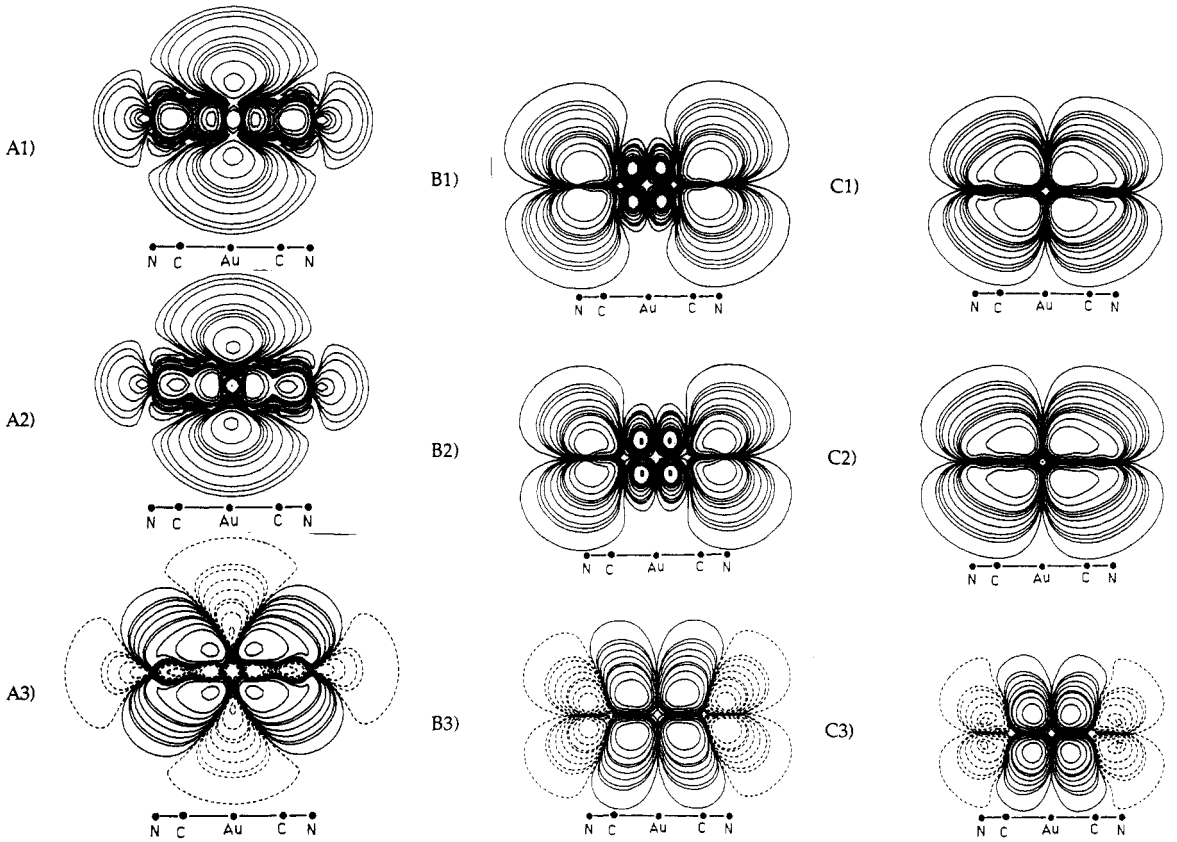

Figure 4. Contours of electron density of $Au(CN)_2^-$. (A) σ_g orbital; (B) $1\pi_g$ orbital; (C) $2\pi_g$ orbital; (1) ρ_{NR}; (2) ρ_R; (3) $\Delta_R\rho = \rho_{NR} - \rho_R$. The bond distances from the relativistic calculation have been taken as given in Tables I and II.

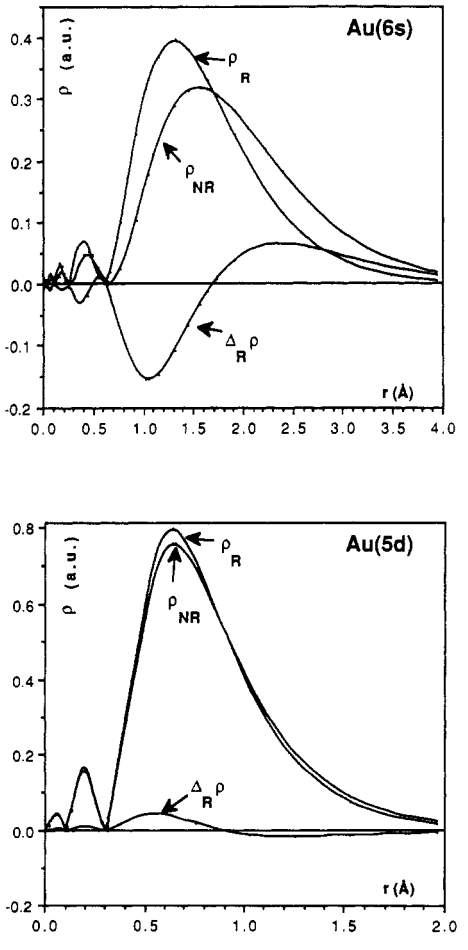

Figure 5. Radial densities for the Au(6s) and spin–orbit-averaged Au(5d) orbitals.

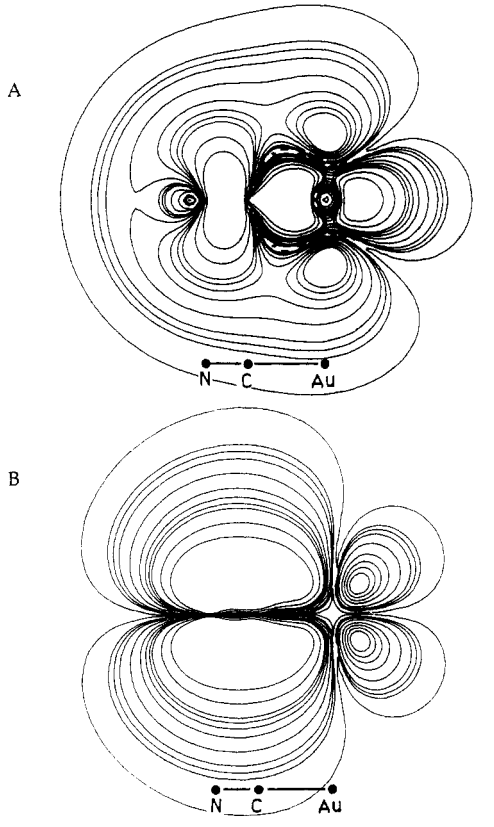

Figure 6. Contours of the relativistic electron density of the (A) σ HOMO and (B) π HOMO of AuCN. The bond distances are given in Tables II and III.

Au–L bond energy in AuL_2^- to be greater than that in AuL.[7] The recently published dissociation energies of CuF and CuF_2^- also show a bond strengthening on adding a second F^- ligand (at the

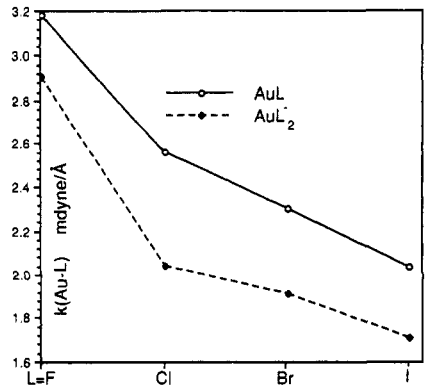

Figure 7. Au–halide stretching force constants for the compounds AuL and AuL_2^-. The force constants are calculated from frequency analyses[37] of experimentally given frequencies[1,44] (if available, or from scaled CI frequencies[7] (Figure 1)).

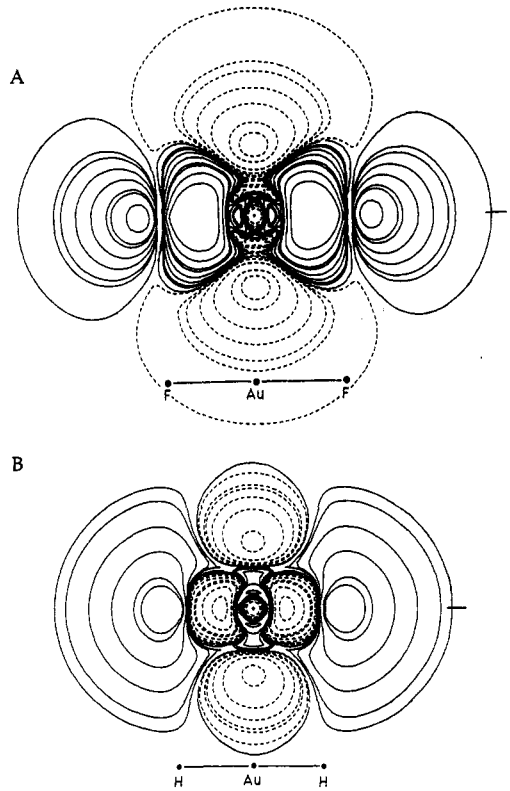

Figure 8. Contours of the relativistic electron difference density of the σ_g HOMO of (A) AuF_2^- at r(Au–F) = 2.1 Å and (B) AuH_2^- at r(Au–H) = 1.8 Å.

CISC level $D_e^1(CuF_2^- \rightarrow CuF + F^-)$ = 430 kJ/mol and D_e^2(Cu–F) = 377 kJ/mol),[30] so this argument does not hold. The same sequence of force constants is seen also at the nonrelativistic level (compare Table I of this work and ref 7); hence, this is not simply a relativistic effect. Decreases in the Au–L stretching force constant from AuL to AuL_2^- are consistent with the calculated increase in the Au–L bond distance. This may also be caused by the more diffuse Au(6s) orbital in the Au–L bond of AuL_2^-.

The Vibrational Analysis of $Au(SCN)_2^-$. The vibrational frequencies of $Au(SCN)_2^-$, measured in this work (see the experimental section III), are substantially in agreement with the previously reported values.[5] A band due to ω(C–S) has been observed at 705–722 cm^{-1} in $KAu(SCN)_2$[6] (split in the solid state) and at 691 cm^{-1} in $[NBu_4]Au(SCN)_2$. It was not seen in the $AsPh_4^+$ salt owing to intense bands of this cation.[3] Comparison of the Raman spectra of $[AsPh_4][Au(SCN)_2]$ and $[AsPh_4][AuCl_2]$ reveals a band at 695 cm^{-1} in the spectrum of the former, which we attribute to ω(C–S). The ω(Au–S) frequencies appear as

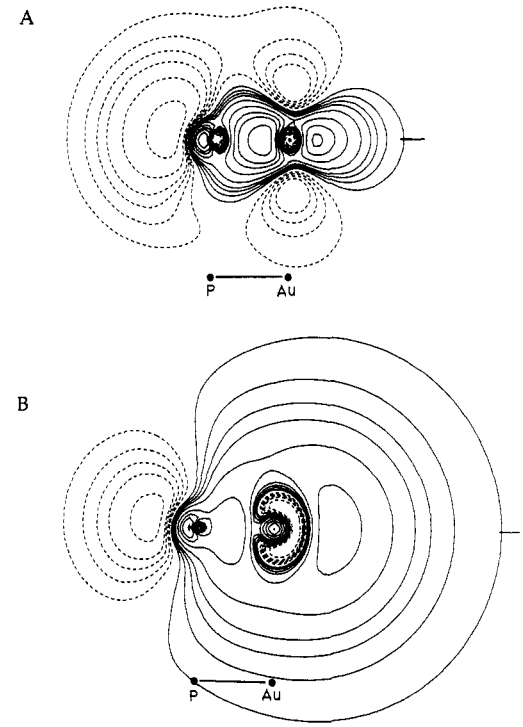

Figure 9. Contours of the relativistic (A) A_1' HOMO, and (B) A_1' LUMO for $AuPH_3^+$. The bond distances and angles are given in Tables II and III.

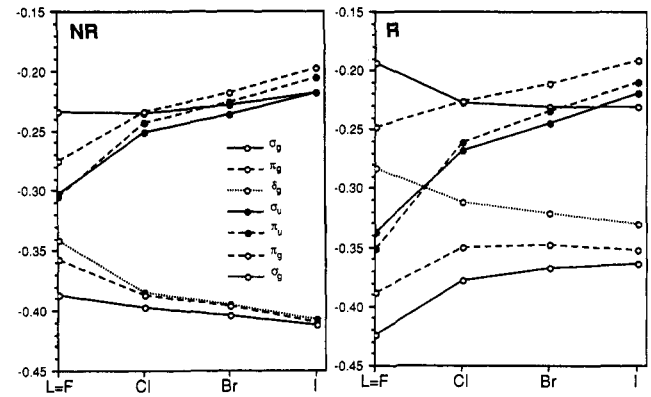

Figure 10. Valence orbital energies for the halide AuL_2^- complexes (L = F, Cl, Br, I). For comparison, orbital energies of the gold atom in the same basis set are as follows (in au): NR, −0.522 (5d), −0.223 (6s); R, −0.463 (5d), −0.290 (6s).

medium-intensity bands at 306 cm^{-1} (Raman) and at 310 cm^{-1} (IR), as expected for a centrosymmetric structure,[2] whereas ω(C–N) stretching has almost the same frequency (2120 cm^{-1}) in Raman and IR spectra. Au–S–C and S–Au–S bending modes are found in the far-IR spectrum at 144 and 110 cm^{-1}, respectively. The S–Au–S bending mode of 110 cm^{-1} is close to the frequency obtained for the same mode in $[Bu_4N][Au(SMe)_2]$ (112 cm^{-1}).[5] Although the vibrational spectra support linear S–Au–S coordination, with little coupling between the modes of the thiocyanate ligands, they are insufficient to determine the extent to which the structure is bent at the sulfur atoms. Relativistic HF calculations predicted the bent configuration of this molecule, and we have confirmed this by a single-crystal X-ray structural determination as discussed before. With the structural data from the solid state, we have been able to perform a harmonic frequency analysis using Wilson's GF matrix method[36] within the program VIB[37] to de-

(36) Wilson, E. B.; Decius, J. C.; Cross, P. C. *Molecular Vibrations, The Theory of Infrared and Raman Vibrational Spectra*; McGraw-Hill: London, 1955.
(37) Schwerdtfeger, P.; Bowmaker, G. A.; Boyd, P. D. W.; Earp, C. D.; Hannon, S. F. VIB. Department of Chemistry, University of Auckland, Auckland, NZ, 1987.

termine the harmonic valence force field. This program optimizes force constants by minimizing the absolute error ϵ of the difference between the observed ω_Γ and calculated frequencies $\tilde{\omega}_\Gamma$ in each irreducible representation Γ of the considered point group $\mathcal{G}$, i.e.

$$\epsilon = \sum_\Gamma \sum_{\omega_\Gamma} |(\omega_\Gamma - \tilde{\omega}_\Gamma)| > 0 \qquad (2)$$

As initial force constants in the fit procedure, we used the force constants of SCN^- given by Jones[38] and our calculated values obtained from the Fletcher–Powell geometry optimization. The optimized force field k_{ij} is given in Table X. Without the nondiagonal force constants listed in Table X, the error ϵ increases from 18 to 53 cm^{-1}. To achieve agreement with experiment, more nondiagonal matrix elements k_{ij} $(i \neq j)$ have to be included. Note that the force constants given in Table X represent the global minimum with respect to ϵ; several local minima with $\epsilon' > \epsilon$ occur with slightly different force constants for the bending modes. This is mainly due to the strongly coupled bending modes. For example, from the potential energy distribution, we obtain a mixture of 60% S–Au–S, 30% Au–S–C, 9% S–C–N bending and 2% Au–S stretching contributions for the 110-cm^{-1} IR band, and for the 144-cm^{-1} IR band we obtain 41% Au–S–C, 39% S–Au–S, 15% S–C–N bending, 4% Au–S, and 1% S–C stretching contributions. This has also been observed for similar compounds. For example, Forster et al.[39] did not achieve a good fit without off-diagonal force constants for $Zn(NCS)_4^{2-}$ due to considerable mixing between the Zn–N–C and the N–C–S bending modes.

Karitonov et al. have argued that resonance structures such as

$$^-S{-}C{\equiv}N \leftrightarrow S{=}C{=}N^- \leftrightarrow {}^+S{\equiv}C{-}N^{2-} \qquad (3)$$

would increase the C–S bond order and that the C–N bond order would decrease by coordination through the S atom when compared to the free SCN^- ion.[40] A frequency analysis for SCN^- has been reported by Jones,[38] who derived the valence force field as k(C–N) = 15.95 mdyn/Å, k(S–C) = 5.18 mdyn/Å and k(S–C–N) = 0.3 mdyn/Å. We obtain an overall decrease in the force field of the thiocyanate ligand in $Au(SCN)_2^-$; hence, the simple resonance model in (3) is not appropriate in this case. Karitonov also pointed out that the metal–sulfur M–S force constant is relatively insensitive to changes in the M–S–C angle.[40] This is observed in our calculation if we compare the HF force constants for the linear and the bent $Au(SCN)_2^-$, which differ only slightly at both the nonrelativistic and relativistic level of the theory. A Mulliken population analysis (Table V) shows that the SCN ligand in $Au(SCN)_2^-$ is partially positively charged (q_{SCN} = +0.1 at the relativistic level). This can be rationalized through the following resonance structures

$$Au{-}S{-}C{\equiv}N \leftrightarrow {}^-Au{=}S^+{-}C{\equiv}N \qquad (4)$$

which is represented by the HOMO of symmetry π_g for the linear and B_g for the bent case (Table XI). However, almost all of the charge donation originates from the σ orbitals and not from the π orbitals of the SCN^- ligand. Hence, the SCN^- ligand acts as a σ donor rather than a π donor, as revealed by the gold $6p_\pi$ and $5d_\pi$ populations (Table V).

The relativistic effects in the HF force constants of $Au(SCN)_2^-$ have been calculated as $\Delta_R k_e$(C–N) = −0.26 mdyn/Å (1.2% of the total relativistic HF value k_e(C–N)), $\Delta_R k_e$(S–C) = −1.02 mdyn/Å (18%), $\Delta_R k_e$(Au–S) = −0.19 mdyn/Å (47%), and $\Delta_R k_e$(Au–S–C) = −0.24 mdyn/Å (52%). Similar effects have been found for the compound AuSCN. This changes the frequencies for $Au(SCN)_2^-$ by $\Delta_R\omega$(C–N) = −29 cm^{-1}, $\Delta_R\omega$(S–C) = −61 cm^{-1}, $\Delta_R\omega$(Au–S) = −91 cm^{-1}, and $\Delta_R\omega$(Au–S–C) = −18 cm^{-1} in the IR spectra ($\Delta_R\omega = \omega_{NR} - \omega_R$) if we use the relative relativistic changes in the force field given in Table X and the relativistic corrections to the molecular structure calculated from Tables I and II. This can be seen in the experimental frequencies for the group 11 thiocyanate complexes. For example, the experimental C–N stretching frequency[2] for $Cu(SCN)_2^-$ is 2085 cm^{-1}, for $Ag(SCN)_2^-$ is 2090 cm^{-1}, and for $Au(SCN)_2^-$ is 2118 cm^{-1} (2091 cm^{-1} corrected to the nonrelativistic level). However, the Raman line assigned to the S–C stretching mode in $Au(SCN)_2^-$ is about 50 cm^{-1} below the line observed for $Ag(SCN)_2^-$ and does not agree with our calculated relativistic increase of about 60 cm^{-1}.[3] Rogers also gives assignments for the M–S–C bending modes, i.e. 168 cm^{-1} for M = Cu and 130 cm^{-1} for M = Ag.[3] Our measured Au–S–C bending mode of 144 cm^{-1} shows the expected increase due to relativistic effects. It would be very useful to obtain nonrelativistic and relativistic force fields from CI calculations, since $\Delta_R k_e$ values can change quite dramatically on inclusion of electron correlation. It was not possible to perform these calculations for $Au(SCN)_2^-$ for the reasons discussed above, but the Møller–Plesset procedure mentioned at the beginning of this section resulted in a symmetric Au–S stretching force constant of 1.839 mdyn/Å at the relativistic level. This is in very good agreement with the Au–S stretching force constant given in Table X from a normal-coordinate analysis of the experimental spectrum. Note that the percent relativistic change in $\Delta_R k_e$ decreases for bonds further from the Au center. From the trend in the metal–sulfur stretching force constants shown in Figure 1, we see that the calculated relativistic increase $\Delta_R k_e$ is probably underestimated at the HF level. Similar effects in $\Delta_R k_e$ have been found recently in the Hg–C stretching mode of $Hg(CH_3)_2$.[41]

The Origin of the Relativistic Increase in Gold–Ligand Force Constants. The overall increase found for Au–L stretching force constant has been related directly to the relativistic bond contraction;[7,8] i.e., the inequality $\Delta_R k_e < 0$ may be a topological effect. However, a detailed quantitative analysis of this effect has still to be done. If we split the total energy of a molecule into its electronic and pure nuclear components (in au)

$$E = E(\text{electronic}) + \sum_{\alpha \neq \beta} Z_\alpha Z_\beta |\mathbf{R}_\alpha - \mathbf{R}_\beta|^{-1} \qquad (5)$$

we obtain the relativistic change in the quadratic Au–L stretching force constant (r is the internal coordinate of the Au–L bond; anharmonic corrections are neglected)[42]

$$\Delta_R k_e(\text{Au–L}) = \Delta_R k(\text{Au–L; electronic}) + 2Z_{Au}Z_L(r_e^{NR} r_e^{R})^{-3}[(r_e^{R})^3 - (r_e^{NR})^3] \qquad (6)$$

The first part in eq 6 arises mainly from relativistic changes in the electronic wave function as well as from the action of the relativistic perturbation operator on the nonrelativistic wave function. The second term in eq 6 is dependent on the relativistic change of the cubic power of the nonrelativistic and relativistic bond distance, which in fact can be quite large for large relativistic bond contractions. Note, that the second term in eq 6 is zero for $r_e^{NR} = r_e^{R}$ and less than zero for $r_e^{NR} > r_e^{R}$. This agrees with $\Delta_R k_e < 0$ calculated in general for Au compounds. Hence, the total electronic part is expected to be positive and smaller than the second term in eq 6 (Z_{Au} = 79 and $Z_L \geq 1$) for large relativistic bond contractions as observed for all gold compounds.[8] This may explain part of the overall increase in force constants. In fact, there is not one case known in gold compounds where stretching force constants decrease whereas bond distances decrease significantly ($\Delta r > 0.1$ Å) due to relativistic effects. For very small relativistic bond contractions or bond expansions, as is the case for $Pb(CH_3)_2^{2+}$,[41] TlH or TlH^+,[43] relativisticly decreased metal–ligand force constants have been calculated recently.[41,43] It has been argued that the Au–L bond is more covalent than the Cu–L and Ag–L bonds, leading to an increased Au–L overlap and therefore an increased bond strength.[1,2] It was shown in the first paper of this series that relativistic effects can increase the

(38) Jones, L. H. *J. Chem. Phys.* **1956**, *25*, 1069.
(39) Forster, D.; Horrocks, W. D. *Inorg. Chem.* **1967**, *6*, 339.
(40) Karitonov, Y. Y.; Tsintsadse, G. V.; Porai-Koshits, M. A. *Russ. J. Inorg. Chem. (Engl. Transl.)* **1965**, *10*, 427.
(41) Schwerdtfeger, P. *J. Am. Chem. Soc.* **1990**, *112*, 2818.
(42) There may also be other routes of partitioning $\Delta_R k_e$ into different contributions which allows different interpretations; see, for example: Rutkowski, A.; Schwarz, W. H. E. *Theor. Chim. Acta* **1990**, *76*, 391.
(43) Schwerdtfeger, P. *Phys. Scr.* **1987**, *36*, 453.
(44) Huber, K. P.; Herzberg, G. *Molecular Spectra and Molecular Structure, Constants of Diatomic Compounds*; Van Nostrand: New York, 1979.

ionicity in the Au–L bond, as the case for the gold–alkali-metal dimers.[7] These compounds also show increased Au–L stretching force constants due to relativistic effects. For the gold halide complexes, the differences in net charges between the gold atom and the halogen ligands decrease due to the increase in the gold EN (Table V). This indicates a larger degree of covalency at least for these compounds, but as shown in Figure 8 for AuF_2^-, electron density is moving out of the bond region into areas perpendicular to the bond axis. This agrees with the fact that $\Delta_R k$(Au–L; electronic) of eq 6 is expected to be positive, but a complete analysis of this electronic term is necessary to understand the origin of the relativistic change in force constants.

C. Bond Stabilities. The HF dissociation energy of the gold compounds as well as the CI calculated values for the gold halides are given in Tables I and III. D_e^1 shows the ability of monodentate Au(I) compounds to add a second ligand. In all cases, we see that Au(I) clearly prefers coordination number 2, and inclusion of relativity in the calculations increases this effect. As a result, the strong energetic destabilization calculated for the diatomic gold halides[7] does not occur in the overall dissociation energy D_e ($\Delta_R D_e$ in Table IV). This tendency of gold to form linear L–Au–L complexes may also be the reason for the polymeric zigzag chains in the gold monohalides, which may be viewed as containing AuL_2^- (L = Cl, Br, I) units.[45] The preference of gold for coordination number 2 also appears at the nonrelativistic level, so relativistic effects may not be the only explanation of the difference in structure between AuCl and AgCl (the latter crystallizes with NaCl structure). A detailed theoretical analysis of the solid state of AuCl and AgCl to explain the structural differences would be of some interest. Nevertheless, relativistic effects support coordination number 2 at the HF level, and we would expect the same trend at the CI level. For example, for AuF_2^-, we get $\Delta_R D_e^1$ = −111.0 kJ/mol at the CI level[9] (−70.7 kJ/mol at the HF level), about 40 kJ/mol larger than the HF value. Hence, correlation effects increase the preference for coordination number 2 in AuF_2^-.

For $AuBr_2^-$ and AuI_2^-, spin–orbit effects in the ligands may become important, and one has to consider such contributions to the dissociation energies.[7,9] For σ bonds, we expect that spin–orbit effects are small at the molecular level compared to the spin–orbit stabilization of the atoms; i.e., $\Delta^{SO}(AuL_2^-) \ll \Delta^{SO}(L)$.[7,9,46] If we therefore neglect molecular spin–orbit contributions, we obtain a spin–orbit destabilization for the AuL_2^- dissociation energy derived from atomic contributions only of Δ^{SO} = 14.7 kJ/mol[46] for L = Br and 30.3 kJ/mol for L = I.[47] The dissociation energies D_e and D_e^2 in Table I have to be corrected by these values, i.e. $D_e^{SO} = D_e - \Delta^{SO}$ (at the CISC level (in kJ/mol) D_e = 487, D_e^2 = 210, ΔD_e^{12} = 67 for $AuBr_2^-$ and D_e = 444, D_e^2 = 176, ΔD_e^{12} = 92 for AuI_2^-). Hence, spin–orbit effects increase the trend to addition of a second ligand in AuL to form AuL_2^-. The ligand spin–orbit contributions of the other gold compounds discussed here are negligible.

For the diatomic compounds, we have been able to relate the relativistic bond stabilizations or destabilizations to the electronegativity of the ligands.[7] This was explained by the relativistic energetic stabilization of the gold valence 6s orbital. Table V shows that this is not possible for the AuL_2^- complexes, since we have an interplay between the relativistic Au(6s) stabilization and the relativistic Au(5d) destabilization, which results in increased Au(5d) contributions to the Au–L bond. In fact, the relativistic stabilization $\Delta_R D_e$ is reversed at the HF level for the gold halides compared to the diatomics,[7] resulting in the sequence of bond stability of the gold halides $AuF_2^- \gg AuCl_2^- \approx AuBr_2^- > AuI_2^-$. This does not reflect the order in stability constants given by Puddephatt.[1] Other (kinetic and solvent) effects play also an important role, so that the bond stabilities cannot be compared directly with stability constants.

We also included AuH_2^- in our calculations for comparison with the other Au(I) complexes. Table I shows that the AuH tends to add H^- to form the as yet unknown complex ion AuH_2^-. It is questionable whether this species can be isolated, but it could perhaps be observed by matrix isolation spectroscopy. Recently, the neutral compound AuH_2 has been investigated theoretically by Balasubramanian and Liao.[48] We therefore give the vertical HF ionization potential to the $^2\Sigma_u^+$ ground state of linear AuH_2: 2.45 eV (NR) and 2.78 eV (R). Hence, this molecule is stable with respect to electron loss, $AuH_2^- \rightarrow AuH_2 + e^-$. Note that the $^2\Sigma_u^+$ state of AuH_2 has been calculated to be only about 0.2 eV below the $^2\Sigma_g^+$ state.[48] The effects of the relativistic increase in the electronegativity of gold (see ref 7) becomes significant for this compound; the gross atomic charge of Au in AuH_2^- decreases from +0.45 at the nonrelativistic level to −0.72 at the relativistic level. The orbital population shows that most of the charge flows from the 1s orbital of H to the 6s orbital of Au. This is also shown in the relativistic difference density $\Delta_R\rho = \rho_{NR} - \rho_R$ plot of the σ_g HOMO of AuH_2^-, Figure 8, together with the σ_g HOMO of AuF_2^-, which describes mainly the bonding in these molecules. The difference density of AuH_2^- shows a density shift from the hydrogen atoms into regions close to the gold atom as expected from the relativistic increase of the gold electronegativity. This is related to the relativistic 6s contraction as well as the relativistic 5d expansion of the gold atom as described above. However, for AuF_2^-, we obtain charge flow only into areas perpendicular to the AuF bonding axis. This may increase the reactivity of this compound in this direction and therefore increase the ability of AuF_2^- to add more ligands forming compounds of higher coordination number. This density shift out of the bonding area may also explain why AuF_2^- has a lower force constant than AuF.

$AuCH_3$ is not very stable at the HF level, and this compound has not been isolated or observed yet. $AuCH_3$ can be stabilized by addition of a second ligand, and complexes of the form $LAuCH_3$ (L = PPh_3, CH_3^-, ...) are well-known.[1] C-bonded gold species, which may appear to contain a single Au–C bond from their empirical formula, are assumed to have a cyclic structure. For example, 2-pyridylgold(I) is assumed to have a cyclic trimeric structure with a Au–N(pyridine) bond.[1] $Au(CH_3)_2^-$ is the least stable compound calculated at the HF level, but it has been isolated by Tamaki and Kochi[49] and by Rice and Tobias.[50] In agreement with our calculated low HF dissociation energies, $Au(CH_3)_2^-$ is extremely unstable and reacts violently with water or methanol.[50] The population analysis in Table V shows that the methyl groups are negatively charged $q(CH_3)$ = −0.54, and therefore may react easily with the counterion M^+. Indeed, Rice and Tobias isolated the compound $Li[Au(CH_3)_2]$ only by chelating the Li^+ cation with PMDT.[50] The low dissociation energies suggest that $Au(CH_3)_2^-$ is thermodynamically unstable (but kinetically stable under certain conditions) and may decompose. This is quite similar to $Hg(CH_3)_2$, which has been studied recently.[41] Also $Ag(CH_3)_2^-$ is not known (a crystal structure of $Cu(CH_3)_2^-$ has been given recently[51] suggesting that relativistic effects are important in explaining the existence of $Au(CH_3)_2^-$. Indeed, relativistic effects stabilize the Au–C bond in $Au(CH_3)_2^-$ by about 34 kJ/mol at the HF level and 39 kJ/mol at the MP2 level.[41] Correlation effects may increase this value and a nonrelativistic CI calculation may show that $Au(CH_3)_2^-$ is not stable toward decomposition into C_2H_6 and other reaction products (see for example the MP2 calculations performed for this compound in ref 41).

The neutral $AuPH_3$ is calculated to be unstable at the HF level with respects to the dissociation into Au + PH_3. This is in agreement with the fact that $AuPR_3$ compounds (R = H, Me, Ph, ...) have never been observed as monomers. In contrast, several cluster compounds of $AuPH_3$[52,53] have been isolated in the past,

(45) Schwerdtfeger, P. Unpublished results.
(46) Schwerdtfeger, P.; Szentpály, L. v.; Vogel, K.; Silberbach, H.; Stoll, H.; Preuss, H. *J. Phys. Chem.* **1986**, *84*, 1606.
(47) Moore, C. E. Atomic Energy Levels. *Natl. Bur. Stand. Circ. (U.S.)* **1958**, *No. 467*.
(48) (a) Balasubramanian, K.; Liao, M. Z. *J. Phys. Chem.* **1988**, *92*, 361. (b) Balasubramanian, K.; Liao, M. Z. *J. Phys. Chem.* **1989**, *93*, 89. (c) Balasubramanian, K. *J. Phys. Chem.* **1989**, *93*, 6585.
(49) Tamaki, A.; Kochi, J. K. *J. Organomet. Chem.* **1973**, *51*, C39.
(50) Rice, G. W.; Tobias, R. S. *Inorg. Chem.* **1975**, *14*, 2402; **1976**, *15*, 489.
(51) Dempsey, D. F.; Girolami, G. S. *Organometallics* **1988**, *7*, 1208.
(52) (a) Steggerda, J. J.; Bour, J. J.; van der Velden, J. W. A. *Recl. Trav. Chim. Pays-Bas* **1982**, *101*, 164. (b) Scherbaum, F.; Grohmann, A.; Huber, B.; Kruger, C.; Schmidbaur, H. *Angew. Chem., Int. Ed. Engl.* **1988**, *27*, 1544.

but we assume that $AuPPh_3$ would not be stable either and would dimerize to the known dinuclear compound $Au_2(PPh_3)_2$.[53,54] Even at the CI level, we obtain a relatively long Au–P bond distance of 2.625 Å (other CI bond distances and angles: r_e(P–H) = 1.456 Å, α_e(Au–P–H) = 120.4° and α_e(H–P–H) = 96.7°) and a very small Au–P stretching force constant of 0.519 mdyn/Å. The singly occupied MO has mainly Au(s) character with little admixture (10%) of P(sp_σ) orbitals; hence, the Au atom seems to be inert for the closed-shell PH_3 ligand. In contrast, $AuPH_3^+$ is calculated to be stable with respect to the dissociation $Au^+ + PH_3$. This dissociation is preferred relative to the other possible dissociation producing $Au + PH_3^+$, since the ionization potential IP of gold is smaller than the IP of PH_3, i.e. IP(Au) = 9.23 eV[47] (7.67 eV at the Dirac–Fock level using the program MCDF)[29] and IP(PH_3) = 9.87 eV[55] (8.73 eV at the HF level using a 6-311G* basis set). Derivatives of $AuPH_3^+$ are well-known; i.e., $AuPPh_3^+ ClO_4^-$ has been isolated.[56] It has been suggested that the $AuPR_3$ fragment (R being any organic ligand) is isolobal with the hydrogen atom.[57] Furthermore, $AuPR_3^+$ may than be seen as isolobal to H^+.[57] Compounds that are isolobal to H_2O [$(AuPR_3)_2O$] (not yet prepared), H_3O^+ [$(AuPR_3)_3O^+$] (prepared[57]), or H_2 [$(AuPR_3)_2$] (prepared[53]) are the subject of current research. According to the isolobal analogy developed by Hoffmann,[59] $AuPR_3^+$ is a simple case since H^+ has no electrons. One may compare the electronaffinities of these compounds: EA(H^+) = 0.5 au, $EA_R(AuPH_3^+)$ = 0.210 au, $EA_{NR}(AuPH_3^+)$ = 0.181 au at the HF level, and $EA_R(AuPH_3^+)$ = 0.217 au at the CISC level (calculated CI geometry of $AuPH_3^+$: r_e(Au–P) = 2.432 Å, r_e(P–H) = 1.438 Å, α_e(Au–P–H) = 114.9°). The calculated electron affinities for $AuPH_3^+$ and H^+ are different, and it will be interesting to see if the isolobal analogy is valid for $AuPR_3^+$ compounds. Nevertheless, we include plots of the A_1' HOMO and LUMO for this complex (Figure 9). The LUMO shows an almost spherical electron density distribution around the Au atom that can be compared with the spherical H(1s) orbital. The Au–P bond is best described by the A_1' HOMO, which shows large Au(5d) contributions. The relativistic change in the tendency of $AuPH_3^+$ to add a second ligand, i.e. $AuPH_3^+ + PH_3 \rightarrow Au(PH_3)_2^+$, is $\Delta_R D_e \sim -100$ kJ/mol, which is relatively large compared with that of the other compounds. The overall relativistic stabilization is $\Delta_R D_e$ = −173 kJ/mol at the HF level. This is probably due to the positive charge in this complex; i.e., there is a charge flow from the PH_3 ligands toward the positively charged gold atom, and the relativistic 6s stabilization leads to an overall increase in the dissociation energy. This may explain the stability of such complexes, since no such compounds are known for copper and very few for silver chemistry.[27]

$Au(SCN)_2^-$ is rather unstable in aqueous solution and rather rapidly undergoes the disproportionation reaction[60]

$$3Au(SCN)_2^- \rightarrow 2Au + Au(SCN)_4^- + 2SCN^- \qquad (7)$$

The reported stability constants of isocyanate complexes are small compared to those with many other ligands.[1] This may be reflected in the very low HF dissociation energies for these complexes when compared for example to the other halides or $Au(CN)_2^-$. At the relativistic level this compound shows a very strong tendency for coordination number 2 (ΔD_e[12] = 145 kJ/mol). This agrees with the fact that the singly bonded gold thiocyanate is observed only together with stabilizing ligands, i.e. LAuSCN, or as a polymeric structure in the solid state with S–Au–S units.[1,60] Also, AuSCN is very unstable and decomposes rapidly above 140 °C to give gold and dithiocyanogen.[60] In contrast, AuCN and $Au(CN)_2^-$ are very stable compounds with relatively large dissociation energies at the HF level compared to all the other calculated compounds (see Table I). This agrees with experimental findings; $Au(CN)_2^-$ is the most stable complex known in Au(I) chemistry and has a very large stability constant in aqueous solution.[1] The analogous decomposition (eq 7) for the cyanide complex is not observed and the gold(III) complex $Au(CN)_4^-$ is less stable than $Au(CN)_2^-$.[1] One reason for the high stability of $Au(CN)_2^-$ is certainly the π bond between the Au(d_π) and the CN(p_π) orbitals as shown in Figure 4 and discussed above. The electron affinity of CN($^2\Sigma^+$) has been calculated to be 2.91 eV at the HF level. (experimental value 3.82 eV[44,61]). The electron affinity calculated for SCN($^2\Pi$) at the HF level is 2.44 eV (experimental value 3.51 eV[62]; the $^2\Sigma^+$ state lies 5.49 eV above the $^2\Pi$ state within the HF approximation).

D. Orbital Energies and Populations. Ligand field theory predicts that the energy ordering of the d orbitals in linear gold complexes should follow the order $d_\sigma \gg d_\pi > d_\delta$.[1] The δ orbitals are expected to be nonbonding. It is clear from the calculations reported here and from those of other workers that this simple model does not give a satisfactory description of these complexes. In particular, the inclusion of Au 6s and 6p orbitals is seen to be essential for a description of the higher lying "ligand field" orbitals. Figure 10 and Table XI give the variation of orbital energies and orbital composition for the series of halide complexes AuX_2^- (X = F, Cl, Br, I) for both the relativistic and nonrelativistic HF calculations. The order of d-orbital energies is $d_\delta > d_\pi > d_\sigma$, as expected from the MO theory. A striking feature of Figure 10 can be seen in a comparison of the results of the two calculations. In the nonrelativistic case the gold d orbitals in the energy range −0.34 to −0.4 au are "corelike", whereas in the relativistic case the relativistic d orbital expansion and s orbital contraction lead to significant s–d mixing. In the case of AuF_2^-, the F(2p) σ_u and π_u orbitals lie lower in energy than the Au(5d) δ_g orbitals, and the core is mixed up with the valence space. Obviously, the s–d mixing is dependent on the electronegativity of the ligand; i.e., we expect a large s–d interaction and a small s–p interaction with electronegative ligands (σ acceptors) and the opposite for electropositive ligands (σ donors). For example, AuI_2^- shows a well-defined separation between the Au(5d) core and the valence space, and the p population in gold is largest. However, AuH_2^- shows also large d as well as p interactions (Table V); hence, it is not possible to obtain general rules about d or p participations for all possible ligands. The trends observed in the relativistic results in Figure 10 are qualitatively similar to those found in nonrelativistic scattered-wave Xα calculations.[13] The main quantitative difference between these two studies lies in the position of the σ_g orbitals (Au(s,d)) relative to the π and δ orbitals. This is expected to be quite sensitive to the amount of s–d mixing. Guenzburger and Ellis[11] have reported a discrete variational calculation on the $AuCl_2^-$ ion. The ordering of orbital energies in this study is the same as that reported here for their relativistic calculation. The amount of Au(5d) and Au(6p) participation in the gold–halogen bond is also reflected in the trend of the σ_g and σ_u HOMOs. While the halogen σ_g HOMO is destabilized by the occupied Au($5d_\sigma$) orbital, the halogen σ_u HOMO is stabilized by the empty Au($5d_\sigma$) orbital. This is clearly seen if we compare the nonrelativistic with the relativistic calculation (Figure 10); i.e., the σ_g–σ_u splitting increases due to relativistic effects, which increase the 5d- and 6p-orbital participation in the Au–L bond.

There have been several studies of the electronic structure of the $Au(CN)_2^-$ ion using scattered wave[8] and discrete variational[12,13] Xα calculations (we should note that the HF–Slater orbital en-

(53) (a) Mingos, D. M. P. *Pure Appl. Chem.* **1980**, *52*, 705. (b) Hall, K. P.; Mingos, D. M. P. In *Progress in Inorganic Chemistry*; Wiley: New York, 1984; Vol. 32, pp 264 and 295.
(54) Schwerdtfeger, P.; Boyd, P. D. W.; Brienne, S.; Burrell, A. K. Manuscript in preparation.
(55) Berkowitz, J.; Curtiss, L. A.; Gibson, S. T.; Greene, J. P.; Hillhouse, G. L.; Pople, J. A. *J. Chem. Phys.* **1986**, *84*, 375.
(56) Uson, R.; Royo, P.; Laguna, A.; Garcia, J. *Rev. Acad. Cienc. Exactas, Fis., Quim. Nat. Zaragoza* **1973**, *28*, 67.
(57) (a) Lauher, J. W.; Wald, K. *J. Am. Chem. Soc.* **1981**, *103*, 7648. (b) Hall, K. P.; Mingos, D. M. P. *Prog. Inorg. Chem.* **1984**, *32*, 237. (c) Bruce, M. Personal communication.
(58) (a) Nesmeyanov, A. N.; Grandberg, K. I.; Dyadchenko, V. P.; Lemenovskii, D. A.; Perelova, E. G. *Izv. Akad. Nauk SSSR, Ser. Khim.* **1974**, 740. (b) Nesmeyanov, A. N.; Perelova, E. G.; Struchkow, Y. T. *J. Org. Chem.* **1980**, *201*, 343.
(59) Hoffmann, R. *Angew. Chem., Int. Ed. Engl.* **1982**, *21*, 711.
(60) Gent, W. L. G.; Gibson, C. S. *J. Chem. Soc.* **1949**, 1835.
(61) Berkowitz, J.; Chupka, W. A.; Walter, T. A. *J. Chem. Phys.* **1969**, *50*, 1497.
(62) Dillard, J. G.; Franklin, J. L. *J. Chem. Phys.* **1968**, *48*, 2353.

ergies are conceptually different compared to those obtained from a HF calculation, since they do not obey Koopmans theorem[63]). The orbital energy ordering found from the HF results differs from both types of calculation. In particular, whereas all three lead to the same HOMOs σ_g and π_g, the ordering of the lower energy orbitals varies particularly from the δ_g(Au(d)) orbital. As this δ orbital is nonbonding, it reflects the energy of the atomic d orbital in the molecular field for each of these calculations. Puddephatt pointed out that the total splitting of the 5d states may not be more than 5000 cm^{-1} and that the 5d electrons are corelike.[1] Mason et al. concluded in their LMCT studies that the Au(5d) electrons are corelike, and they support sp-hybridization for the Au(I) complexes.[16] Since we find large CN(sp)–Au(sd) mixings for the σ_g orbitals, it is difficult to identify the nature of the Au(d_σ) orbital. We therefore chose the Au(5d) δ_g–π_g orbital energy ligand field splitting, which is very small at the nonrelativistic level (~500 cm^{-1}) but large at the relativistic level (~8500 cm^{-1}). The δ_g–π_g separation given by Guenzburger and Ellis derived from HF–Slater calculations (~6000 cm^{-1}) is smaller than our value. This suggests that the 5d electrons are not corelike as is the case for AuF_2^- (Figure 10). We have neglected spin–orbit coupling, which is very important for the Au(5d) electrons. A MCDF calculation[29] shows a separation of ~14 200 cm^{-1} between the $5d_{5/2}$ and the $5d_{3/2}$ orbitals. However, the spin–orbit splitting in the π_g and δ_g levels may be slightly quenched by the molecular field, as is the case for $Hg(CN)_2$.[15] To obtain a measure of such effects, we have calculated the spin–orbit averaged vertical ionization potential of $Au(CN)_2^-$ for the $5d_\delta$ state, i.e. $^1\Sigma_g^+(Au(CN)_2^-) \rightarrow {}^2\Delta_g(Au(CN)_2)$. At the relativistic HF level, we obtain 6.35 eV, in poor agreement with Koopmans energy of 9.22 eV (Table XI). However, this value is still too large compared with the value of 5.2 eV obtained from XPS measurements;[12] the difference is due to correlation and spin–orbit effects. For example, if we assume that the spin–orbit splitting for the 5d electrons is not influenced by the molecular field, we obtain a correction for the $5d_\delta$ ionization of ~1.1 eV ("$5d_{5/2}$") from the splitting in the orbital energies calculated for the neutral gold atom with the program MCDF.[29] This lowers the HF ionization energy to 5.3 eV, which is in now in excellent agreement with the XPS measurements. By use of this approximation, the other spin–orbit-coupled peak should occur at about 7.1 eV ("$5d_{3/2}$"), which may be identified with the left shoulder of the main peak in Sano's XPS spectrum of $Au(CN)_2^-$.

Table V reports the Mulliken orbital populations and atomic charges for all of the Au(I) complexes studied here. For the series of complex halides AuX_2^-, the Au(6s) population ranges from 0.8 to 0.95 for X = F to I. This is also found in previous scattered-wave Xα calculations.[11] There is also a small population of the Au($6p_\sigma$) orbital (0.15–0.33, F–I). In the case of the $Au(CN)_2^-$ ion relativistic calculations show a large Au(6s) population and a decreased Au(sd) population relative to the halide AuL_2^- complexes. This appears to be due to an increased interaction of the Au(6s) orbital with the cyanide σ-donor orbitals, which are at lower energies than the corresponding halide p_σ orbitals and hence are closer in energy to the Au(6s) σ orbital. Similar effects have been noted in the Xα calculations for this complex. The Au(5d) population follows the order of decreasing electronegativity in the halide complexes; i.e., F > Cl > Br > I. This is expected from the s–d mixing shown in Figure 10. Previous Mössbauer and NQR spectroscopic methods supported p rather than d participation in the Au–L bond. This, however, is seen by us to be due to these methods used, which are more sensitive to small changes in densities of p compared to d symmetries, as shown for example in an analysis of the ^{197}Au NQCC in Au(I) complexes by Bowmaker et al. using MSXα calculations.[13]

Due to the positive charge of $Au(PH_3)_2^+$, the PH_3 ligand acts as a strong σ donor (Table VI). This effect has also been observed in ^{197}Au NQCC of compounds containing PPh_3 ligands, e.g. $(PPh_3)_2AuCl$ and $(PPh_3)AuCl$.[2] It is interesting to show the relativistic changes in the ligand charges in $Au(SCN)_2^-$: (NR) $Au^{0.49+}$ $S^{0.45-}$ $C^{0.19+}$ $N^{0.48-}$; (R) $Au^{0.23-}$ $S^{0.02-}$ $C^{0.05+}$ $N^{0.42-}$. As expected, we get a very large change in the atomic charge at the sulfur and small changes at the carbon and nitrogen atom. Large changes in the Au–L charge distribution should also change significantly the reactivity of such compounds, and investigations in this direction would be very interesting.

E. ^{35}Cl Nuclear Quadrupole Coupling in $AuCl_2^-$. Nuclear quadrupole coupling frequencies for ^{35}Cl and ^{197}Au in compounds of the formula LAuCl have been reported and discussed previously.[64] We are interested in changes in the nuclear quadrupole coupling constant (NQCC) of chlorine caused indirectly by relativistic effects in the gold atom. This can be expected to be quite large since electric field gradients (EFG) can be quite sensitive to small changes in the electron density around the metal–ligand center.[13] For example, the measured ^{35}Cl NQCC in CuCl (–32.3 MHz) is quite similar to the one in AgCl (–36.5 MHz).[13] However, the NQCC in $CuCl_2^-$ (–19.3 MHz) differs quite significantly from the measured value for $AuCl_2^-$ (–35.2 MHz). The total relativistic effect in the EFG q ($=q_\sigma$), $\Delta_R q$, may be split into two important contributions

$$\Delta_R q = \{q^{NR}(r_e^{NR}) - q^R(r_e^{NR})\} - \{q^R(r_e^R) - q^R(r_e^{NR})\} = \Delta q_1 - \Delta q_2 \quad (8)$$

The second part of eq 8, Δq_2, describes the change in the EFG due to the difference in the metal–ligand bond distance given by the amount of the relativistic bond contraction, whereas the first term, Δq_1, includes the relativistic change in the electronic structure at a fixed metal–ligand bond distance, in this case the nonrelativistic bond distance r_e^{NR}. For $AuCl_2^-$, we have calculated the following chlorine EFGs (in au): q^R = –1.496 (experimental –1.827), q^{NR} = –0.808, and the differences Δq_1 = +0.671 and Δq_2 = –0.017, resulting in a total $\Delta_R q$ of +0.688. The distances r_e^{NR} and r_e^R have been taken from Table I. The second term in eq 8 is very small, which means that the NQCC is not very sensitive to changes in the internuclear distance; i.e., we have calculated for the EFG derivatives $\delta q = \partial q/\partial r$ (in au/Å): $\delta q^R(r_e^R)$ = 0.286, and $\delta q^{NR}(r_e^{NR})$ = –0.061. It is now interesting to compare the ^{35}Cl NQCC for the group 11 halide complexes MCl_2^-: M = Cu, –19.3 MHz;[13] M = Ag, –13.9 MHz (from all-electron HF results at an optimized bond distance of r_e(Ag–Cl) = 2.529 Å);[45] M = Au, –35.2 MHz (corrected nonrelativistic value, NQCC(exp) + Δ_RNQCC, –21.9 MHz; calculated nonrelativistic HF NQCC, –15.6 MHz). The relativistic HF ^{35}Cl NQCC of –28.8 MHz in $AuCl_2^-$ overestimates the experimental value by about 6.4 MHz. Similar errors have been found by using the scattered-wave Xα method. Hence, the ^{35}Cl NQCC in $AgCl_2^-$ is probably also overestimated, and the experimental value for this compound is expected to be very similar to that for the copper species. The reason for this is the neglect of electron correlation and the limited basis sets used in our calculations. Also the value for $\Delta_R q$ may increase with the inclusion of electron correlation. To conclude, the difference in ^{35}Cl NQCC between $CuCl_2^-$ and $AuCl_2^-$ is mainly due to relativistic effects. A detailed analysis of these compounds using CI methods would be very useful; very large relativistic effects are also expected for the ^{197}Au NQCC. Such effects have not yet been investigated.

III. Computational and Experimental Details

Computational Details. The methods used have been described in detail in refs 7 and 65. Multielectron adjusted nonrelativistic and relativistic pseudopotentials with a small core definition for gold, i.e. a [Xe4f^{14}] core for gold defining the (5s5p5d6s) orbitals as the valence space, were used. The nonrelativistic and relativistic pseudopotentials and basis sets for gold, bromine, and iodine are given in ref 7. For C, N, S, and P we used a 6-311G* basis set.[66] A diffuse s function for N with exponent 0.02 was added to obtain better results for the negatively

(63) Noodleman, L.; Post, D.; Baerends, E. J. *Chem. Phys.* **1982**, *64*, 159

(64) (a) Jones, P. G.; Williams, A. F. *J. Chem. Soc., Dalton Trans.* **1977**, 1430. (b) Jones, P. G.; Maddock, A. G.; Mays, M. J.; Muir, M. M.; Williams, A. F. *J. Chem. Soc., Dalton Trans.* **1977**, 1434. (c) McAuliffe, C. A.; Parish, R. V.; Randall, P. D. *J. Chem. Soc., Dalton Trans.* **1977**, 1426.

(65) Schwerdtfeger, P.; Boyd, P. D. W.; Bowmaker, G. A.; Mack, H. G.; Oberhammer, H. *J. Am. Chem. Soc.* **1989**, *111*, 15.

charged species CN^- and SCN^-. Our method is comparable in quality to the all-electron spin-orbit averaged relativistic HF procedure using relatively large basis sets.[7] The geometries are fully optimized by using a Fletcher-Powell procedure within the GAUSSIAN86 program.[66] It should be noticed that HF dissociation energies and force constants are not very accurate compared to experimental results, because of neglect of electron correlation. However, HF properties are certainly useful for discussing trends. We therefore carried out configuration interaction calculations with single and double substitutions (CISD; abbreviated to CI in the text) corrected by size-consistency effects[66] (CISD/SC; abbreviated to CISC) for the gold halide complexes. These data have been used for a detailed vibrational analysis[37] of the gold-halogen bond. The CISD orbital range was truncated to about 75 functions but included the (5s5p5d) core of gold in the active orbital space (orbital-energy range -10 to +10 au). Open-shell cases have been treated unrestricted (UHF). A one-point CI calculation for $AuCl_2^-$ required about 9 h of CPU time on a IBM3081 computer. The basis set used for the calculations of $Au(SCN)_2^-$ was quite large, i.e. 275 Gaussians contracted to 142 basis functions. This produced about 23 million two-electron integrals. A one-point HF calculation required about 2 h; the total Fletcher-Powell geometry optimization required about 70 h of CPU time on a IBM3081 computer. The density plots were determined by using the program MOLPLOT.[67]

Experimental Details. Preparation. $[AsPh_4][Au(SCN)_2]$ and $[AsPh_4][AuCl_2]$ were prepared by the procedures described in refs 3 and 5. $[AsPh_4][Au(SCN)_2]$ was recrystallized from ethanol/water to give fine needles. The purity of the $[AsPh_4][Au(SCN)_2]$ samples was confirmed by ^{13}C NMR spectroscopy, with only resonances attributable to the phenyl ring of $[AsPh_4]$ and the carbon of the SCN group being observed.

^{13}C NMR Data. $[AsPh_4]$, 135.0, 133.0, 132.8, 131.4 ppm; SCN, 120.4 ppm (recorded on a Bruker AM-400 NMR spectrometer in $CDCl_3$ at 100.6 MHz and referenced to TMS).

Vibrational Spectra. Raman spectra of $[AsPh_4][Au(SCN)_2]$ as crystals and in CH_2Cl_2 solution were recorded with a Jasco R300 spectrometer using Ar^+ 514-nm laser excitation. IR spectra were measured with Perkin-Elmer 597 (4000-200 cm^{-1}) and Digilab FTS 60 (500-50 cm^{-1}) instruments. The spectra of $[AsPh_4][Au(SCN)_2]$ were compared with those of $[AsPh_4]AuCl_2$ so as to identify the frequencies of the complex anion. The following frequencies were found for $Au(SCN)_2^-$ (see also Table X). Raman bands: 100 m, 108 sh, 306 m (306 m, pol), 450 vw, 695 w, 2120 s (2118 s, pol) cm^{-1}. IR bands: 95 sh, 110 m, 138 sh, 144 m, 302 w, 310 m, 2120 s (2120 s) cm^{-1} (CH_2Cl_2 solution values are given in parentheses).

X-ray Structure Determination. Crystals suitable for X-ray analyses were grown from an ethanol/water solution. The cell parameters were determined by least-squares refinement of 25 accurately centered reflections in the range $5° < 2\theta < 34°$. Crystal stability was monitored by recording three check reflections (800; 040; 008) every 100 reflections, and no significant variations were observed. The data were corrected for Lorentz and polarization effects and an empirical absorption correction was applied, based on ψ-scan data and crystal dimensions ($T_{max} = 0.735$; $T_{min} = 0.460$). A Patterson synthesis revealed the positions of the two heavy atoms, and the remaining non-hydrogen atoms were located by using Fourier maps. Hydrogen atoms were inserted at calculated positions by using a riding model with thermal parameters equal to 0.039 Å^2. Anisotropic thermal parameters were assigned to all non-hydrogen atoms, and the refinement on 150 least-squares parameters converged with $R = 0.037$, $R_w = 0.041$ (Table IX), and a maximum shift/error ratio of 0.05. The final difference map showed no features greater than those reasonably assignable to hydrogen atoms. The function minimized in the refinement was $\sum w(|F_o| - |F_c|)^2$ where $w = [\sigma^2(F_o) + 0.0062F_o^2]^{-1}$. A table of observed and calculated structure factors is given in the supplementary material.

IV. Summary

The main conclusions resulting from our calculations on linear Au(I) complexes are as follows.

(a) All gold(I) compounds studied here show a tendency to form linear complexes with coordination number 2. Relativistic effects increase this trend. This, for example, results in the sequence of bond stability $AuF_2^- \gg AuCl_2^- \approx AuBr_2^- > AuI_2^-$, which is the reverse of the sequence shown for the monohalides.[7] This trend is also followed by the gold-halogen stretching force constants. However, the dissociation energy per Au-L bond of the gold(I) complex halides if compared to the monohalides follows $AuL_2^- > AuL$ in contrast to the force constants, which also shows up at the nonrelativistic level of the theory.

(b) AuSCN and $Au(SCN)_2^-$ are calculated to have a bent Au-S-C structure in agreement with the X-ray structure of $[AsPh_4]Au(SCN)_2$. Relativistic effects strongly increase the stability of the bent Au-S-C arrangement compared to the linear one, by more than 120 kJ/mol per Au-S bond. IR and Raman measurements have been carried out to determine the force field of this compound. The trend in the group 11 metal-sulfur stretching force constants follow the trend observed for all the other Au(I) complex compounds, $k_e(Au-L) > k_e(Cu-L) > k_e(Ag-L)$, due to the relativistic increase in the gold-ligand force constant. A qualitative analysis of the origin of this effect has been given, pointing out the importance of the relativistic bond contraction, which increases the nuclear-nuclear repulsion in the molecular Hamiltonian.

(c) All calculated complexes of gold show an increased negative atomic charge at the gold atom due to the relativistically increased electronegativity of about 0.4[7] for the gold atom. This effect may also be the reason for the tendency of gold to form very stable ylide complexes, e.g. $R_3P^+-CH_2-Au^--CH_3$. Theoretical investigations in this direction are currently underway.

(d) At the nonrelativistic level the 5d electrons are almost corelike. Due to the relativistic 5d-expansion as well as the relativistic 6s contraction, we observe a considerable s-d mixing. This should be revealed in UV and photoelectron spectroscopy of Au(I) complexes, for which we included a list of orbital energies (Table XI). The limitation of using the spin-orbit-averaged orbital energies has been discussed for the $^1\Sigma_g^+(Au(CN)_2^-) \rightarrow {}^2\Delta_g(Au(CN)_2)$ ionization. Electronegative ligands (σ acceptors) support d participation while electropositive ligands (σ donors) support p participation in the gold-ligand bond. Therefore, the preference of sp or sd "hybridization" depends on the nature of the ligand and the coordination number. Malli's statement given recently,[68] "It is safe to state that the $6p_{1/2}$ and $6p_{3/2}$ Dirac-Fock AOS are not involved in gold chemistry," is certainly not true. This paper shows that the differences to the simple diatomic gold compounds[7] are quite significant, and one must be very careful in making conclusions from diatomics to the whole gold chemistry.

(e) Relativistic effects in the ^{35}Cl NQCC in $AuCl_2^-$ are very large; i.e., at the HF level the EFG of chlorine increases by more than 85%. Relativistic effects in NQCCs have not been studied before, except for CuF[30] and some diatomics for the first and second period of the period table.[69] Also, chemical shifts in NMR and isomer shifts in Mössbauer spectroscopy may be sensitive to relativistic changes in the molecular electron density. Such effects have not yet been studied.

In this article, we tried to point out the importance of relativistic effects in the chemistry of linear two-coordinated Au(I) complexes. To obtain more accurate results for the molecular properties discussed here, spin-orbit effects and electron correlation on a more sophisticated level (e.g. MCSCF) have too be taken into account. This has been done, for example, for a series of diatomic molecules by Balasubramanian and co-workers.[48] However, we do not expect large changes in the trends discussed in this work. Besides such calculations on diatomic gold compounds,[7,8] there have been only a few developments on theoretical aspects in the chemistry of gold. We hope that this paper may stimulate further theoretical investigations on relativistic effects in gold chemistry.

(66) (a) Frisch, M. J.; Binkley, J. S.; Schlegel, H. B.; Raghavachari, K.; Melius, C. F.; Martin, L.; Stewart, J. J. P.; Bobrowicz, F. W.; Rohlfing, C. M.; Kahn, L. R.; DeFrees, D. J.; Seeger, R.; Whiteside, R. A.; Fox, D. J.; Fluder, E. M.; Pople, J. A. GAUSSIAN86, Carnegie-Mellon Quantum Chemistry Publishing Unit: Pittsburgh, PA, 1984; extended for local and nonlocal pseudopotentials by P. Schwerdtfeger using PSEPOT for the latter: Kolar, M. *Comput. Phys. Commun.* **1981**, *23*, 275. (b) Pople, J. A.; Seeger, R.; Krishnan, R. *Int. J. Quantum Chem., Symp.* **1977**, *11*, 149. (c) Fletcher, R.; Powell, M. J. D. *Comput. J.* **1963**, *6*, 163.

(67) Lichtenberger, D. L.; Fenske, R. F. MOLPLOT. Quantum Chemistry Program Exchange, Program No. 284.

(68) Malli, G. L. In *The Challange of d and f Electrons, Theory and Computation*; Salahub, D. R., Zerner, M. C., Eds.; American Chemistry Society: Washington, DC, 1989; p 305.

(69) Sundholm, D. Thesis, University of Helsinki, Helsinki, 1985.

Acknowledgment. We are very grateful to IBM New Zealand Ltd. for providing large amounts of computer time. P.S. is very indebted to the Alexander von Humboldt-Stiftung for a FEODOR-LYNEN scholarship and for financial support. Thanks are due to Michael Dolg for providing part of the basis sets and pseudopotentials and to the Auckland University Grants Committee for partial support of this project. We also thank Martin A. Bennett, Ralph Cooney, and Graham A. Bowmaker for their interest in this work and very helpful comments, Cliff Rickard for his help in preparing the X-ray data, and Laurie P. Aldridge for critically reading this paper.

Registry No. $[AsPh_4]Au(SCN)_2$, 128444-83-7; AuH_2^-, 128444-80-4; $Au(CH_3)_2^-$, 57444-56-1; $Au(CN)_2^-$, 14950-87-9; $Au(SCN)_2^-$, 16073-82-8; $Au(PH_3)_2^+$, 128470-26-8; AuF_2^-, 55031-54-4; $AuCl_2^-$, 21534-24-7; $AuBr_2^-$, 23000-74-0; AuI_2^-, 23000-72-8; AuSCN, 128444-78-0; $AuCH_3$, 128444-79-1; AuCN, 506-65-0; $AuPH_3$, 128444-81-5; $AuPH_3^+$, 128444-82-6.

Supplementary Material Available: A table of observed and calculated structure factors for $[AsPh_4]Au(SCN)_2$ (7 pages). Ordering information is given on any current masthead page.

Contribution from the Department of Chemistry, University of California, Berkeley, California 94720

M{hydrotris(3-phenylpyrazol-1-yl)borate}$_2$: Sterically Encumbered Iron(II) and Manganese(II) Complexes

David M. Eichhorn and William H. Armstrong*

Received August 28, 1989

The sterically congested complexes $M(tppb)_2$ (M = Fe, Mn; tppb = hydrotris(3-phenylpyrazol-1-yl)borate) were isolated in good yields from reaction mixtures containing 1 equiv of $M(CF_3SO_3)_2$ and 2 equiv of Ktppb. The iron complex $Fe(tppb)_2$ (**1**) crystallizes in the monoclinic space group $P2_1/n$ with a = 12.896 (3) Å, b = 19.547 (3) Å, c = 21.260 (8) Å, β = 94.03 (1)°, V = 5346 (4) Å^3, and Z = 4. The manganese analogue $Mn(tppb)_2$ (**2**) crystallizes in the orthorhombic space group *Ibca* with a = 19.664 (6) Å, b = 22.271 (8) Å, c = 23.680 (5) Å, V = 10371 (6) Å^3, and Z = 8. The M-N bond lengths in compounds **1** and **2**, particularly for **1**, are markedly longer than corresponding lengths for complexes of less sterically demanding poly(pyrazolyl)borate ligands. The magnetic properties of **1** and **2** are typical of S = 2 and $S = {}^5/_2$ species, respectively. The most dramatic difference between the properties of **1** and **2** and their less sterically hindered counterparts lies in their electrochemical behavior. For example, the Fe^{III}/Fe^{II} reduction potential for **1** is approximately 0.6 V more positive than for $Fe(HB(pz)_3)_2$ ($HB(pz)_3$ = hydrotris(pyrazol-1-yl)borate).

Introduction

The use of tris(pyrazolyl)borate ligands has become increasingly popular in synthetic inorganic, bioinorganic, and organometallic chemistry.[1a] As facially capping tridentate nitrogen donors, they have been used as a convenient substitute for cyclopentadienyl ligands, forming complexes which often demonstrate properties similar to their cyclopentadienyl counterparts.[1b] In bioinorganic chemistry, the tris(pyrazolyl)borates have been used as mimics for imidazole coordination in models for active sites of metalloenzymes.[2] One of the problems encountered in the use of tris(pyrazolyl)borates is their propensity to form ML_2 complexes with transition metals. In order to prevent or retard the formation of such complexes, tris(pyrazolyl)borate ligands with substitution at the 3- and 5-positions of the pyrazole rings have been employed.[3,4]

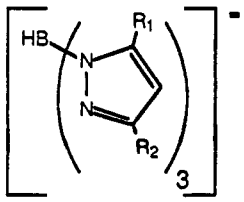

tppb : R_1 = H, R_2 = C_6H_5

The most commonly used of such ligands, hydrotris(3,5-dimethylpyrazol-1-yl)borate, will form ML_2 complexes, but not as readily as the unsubstituted ligand.[3a] Recent reports have described the synthesis and complex formation of the significantly more bulky ligand hydrotris(3-phenylpyrazol-1-yl)borate (tppb), which forms stable complexes of the type ML(SCN)(THF) (M = first-row transition elements), and it was postulated that this ligand would not allow ML_2 formation.[4] As part of our efforts toward modeling the active sites of non-heme iron-containing oxygenases, we were interested in using this ligand to prevent formation of ML_2 complexes. In marked contrast to previous results, we discovered that although formation of MLX complexes is possible, in the absence of strongly coordinating anions the ML_2 complex is formed preferentially. Even when a 1:1 ligand:metal ratio was employed, the ML_2 product was isolated. We report here the syntheses, structures, and properties of the remarkably sterically encumbered $M(tppb)_2$ (M = Fe, Mn) complexes.

Experimental Section

General Procedures. Unless otherwise stated, all materials were used as received without further purification. When dry, degassed solvents are specified, they were distilled from potassium/benzophenone ketyl (THF),[5] sodium (hexanes), or CaH_2 (CH_2Cl_2) and degassed by purging

(1) (a) Trofimenko, S. *Prog. Inorg. Chem.* **1986**, *34*, 115. (b) Trofimenko, S. *Inorg. Chem.* **1969**, *8*, 2675.
(2) (a) Armstrong, W. H.; Spool, A.; Papaefthymiou, G. C.; Frankel, R. B.; Lippard, S. J. *J. Am. Chem. Soc.* **1984**, *106*, 3653. (b) Thompson, J. S.; Marks, T. J.; Ibers, J. A. *J. Am. Chem. Soc.* **1979**, *101*, 4180.
(3) (a) Cleland, W. E.; Barnhart, K. M.; Yamanouchi, K.; Collison, D.; Mabbs, F. E.; Ortega, R. B.; Enemark, J. H. *Inorg. Chem.* **1987**, *26*, 1017. (b) Trofimenko, S.; Calabrese, J. C.; Domaille, P. J.; Thompson, J. S. *Inorg. Chem.* **1989**, *28*, 1091.
(4) Trofimenko, S.; Calabrese, J. C.; Thompson, J. S. *Inorg. Chem.* **1987**, *26*, 1507.
(5) Abbreviations used in this paper: THF, tetrahydrofuran; tppb, hydrotris(3-phenylpyrazol-1-yl)borate; $HB(Me_2pz)_3$, hydrotris(3,5-dimethylpyrazol-1-yl)borate; $HB(pz)_3$, hydrotris(pyrazol-1-yl)borate; tacn, 1,4,7-triazacyclononane; SSCE, saturated sodium calomel electrode; SCE, saturated calomel electrode; NHE, normal hydrogen electrode; TMS, tetramethylsilane; 2-Mephen, 2-methyl-1,10-phenanthroline; MeIm, *N*-methylimidazole; bpy, bipyridyl; terpy, terpyridine; bbt, 2-bis[(2-benzimidazolylmethyl)amino]ethanol; TPP, 5,10,15,20-tetraphenylporphyrinate; EDTA, ethylenediaminetetraacetate; [16]aneN$_5$, 1,4,7,10,13-pentaazacyclohexadecanate; ibz, *N*,*N*-bis(2-benzimidazolylmethyl)amine; $TPP(CN)_3$, 3,8,13-tricyano-5,10,15,20-tetraphenylporphyrinate; $(TPP)Br_4$, 3,8,13,18-tetrabromo-5,10,15,20-tetraphenylporphyrinate $TPP(CN)_4$, 3,8,13,18-tetracyano-5,10,15,20-tetraphenylporphyrinate; dtne, 1,2-bis(1,4,7-triaza-1-cyclononyl)ethane; Fc, ferrocene; phen, 1,10-phenanthroline; Mesaldpt, 1,9-bis(2-hydroxybenzylidene)-1,5,9-triazanonanate; Pctad, bis(2-pyrrolidylidene)-1,5,8,12-tetraazadodecanate; Saltad, 1,12-bis(2-hydroxybenzylidene)-1,4,9,12-tetraazadodec-6-enate; py-pentaamine, 3,6,10,13,19-pentaazabicyclo[13.3.1]nonadeca-1(19),15,17-triene; PhIO, iodosobenzene; MCPBA, *m*-chloroperoxybenzoic acid.

0020-1669/90/1329-3607$02.50/0